



Thermal model of highway overpass bridge  
by Tylar Paul Bunger

A thesis submitted in partial fulfillment of the requirements for the degree of Master of Science in  
Mechanical Engineering  
Montana State University  
© Copyright by Tylar Paul Bunger (2003)

**Abstract:**

A model was developed to calculate the time varying temperature of a highway overpass bridge. This model geometry was drawn using a three-dimensional CAD program, which was also used to discretize the model's geometry into a mesh. This meshed geometry was then imported into RadThemVRT for thermal analysis. RadThemVRT is a multi-mode finite differencing heat transfer code. Conduction, wind convection, solar radiation which can account for shadowing and long wave radiation are the heat transfer modes accounted for by the software. The meshed geometry had material properties assigned to it, including; density, specific heat and thermal conductivity. In addition surface properties were applied, including; emissivity and absorptivity. Emissivity is a measure of how well a body emits thermal radiation and absorptivity is a measure of how well a body absorbs thermal radiation. In addition an instrumentation and data acquisition system were developed for measuring model inputs. Model inputs measured were; air temp (deg C), wind speed (m/s), wind direction (deg), barometric pressure (mmhg), relative humidity (%), total global solar radiation flux (W/m<sup>2</sup>), diffuse solar radiation (W/m<sup>2</sup>) and sky temperature (deg C). These values were measured over extended time periods, with five minute time steps. These inputs were then formatted for input into RadThemVRT. In addition to these parameters a single non-contact surface temperature was measured on the bridge deck (deg C) for use in comparing to the computer solution. A convergence study was also performed to analyze how mesh size and settings in RadThemVRT affect the accuracy of the solution. Two parameters were varied; the size of the elements used in the bridge mesh and a setting used in the program for calculation of view factors. Results of the convergence study reinforce the idea that the accuracy does increase with increasing the number of elements and increasing the view factor settings. The overall accuracy of the model was found to be adequate to justify further study and development of model. The overall conclusion is that the model is accurate in modeling the time varying surface temperature conditions that a bridge deck experiences.

THERMAL MODEL OF HIGHWAY OVERPASS BRIDGE

by

Tylar Paul Bungler

A thesis submitted in partial fulfillment  
of the requirements for the degree

of

Master of Science

in

Mechanical Engineering

MONTANA STATE UNIVERSITY – BOZEMAN  
Bozeman, Montana

August, 2003

N378  
B883

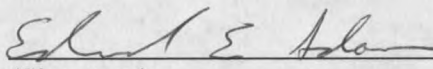
APPROVAL

of a thesis submitted by

Tylar Paul Bunger

This thesis has been read by each member of the thesis committee and has been found to be satisfactory regarding content, English usage, format, citations, bibliographic style, and consistency, and is ready for submission to the College of Graduate Studies.

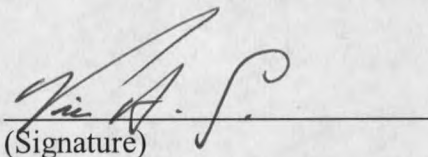
Dr. Edward Adams

  
(Signature)

3-5-03 -2003  
Date

Approved for the Department of Mechanical and Industrial  
Engineering

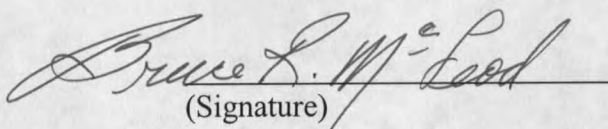
Dr. Vic Cundy

  
(Signature)

9/3/03  
Date

Approved for the College of Graduate Studies

Dr. Bruce R Mcleod

  
(Signature)

9-8-03  
Date

## STATEMENT OF PERMISSION TO USE

In presenting this thesis in partial fulfillment of the requirements for a master's degree at Montana State University – Bozeman, I agree that the library shall make it available to borrowers under rules of the Library.

If I have indicated my intention to copyright this thesis by including a copyright notice page, copying is allowable only for scholarly purposes, consistent with "fair use" as prescribed in the U.S. Copyright Law. Requests for permission for extended quotation from or reproduction of this thesis (paper) in whole or in parts may be granted only by the copyright holder.

Signature Tyler Boyer

Date September 3 2003

© COPYRIGHT

by

Tylar Paul Bungler

2003

All Rights Reserved

## ACKNOWLEDGEMENTS

I would like to thank my advisor Dr. Ed Adams for his guidance and advising. I would also like to thank Ladean McKittrick whose help made this thesis possible.

## TABLE OF CONTENTS

1. INTRODUCTION .....	1
2. BACKGROUND .....	12
CURRENT THERMAL MAPPING.....	12
RADTHERM/RT .....	13
INSTRUMENTATION.....	15
Coastal Environmental WEATHERPAK.....	16
Licor pyranometer.....	16
Epply PIR.....	19
Handheld Infrared Thermometer.....	20
MATERIAL PROPERTIES.....	21
Specific Heat.....	21
Thermal Conductivity.....	23
Density.....	24
Thermal diffusivity.....	24
SURFACE PROPERTIES.....	24
Emissivity.....	25
Absorptivity.....	25
GOVERNING EQUATIONS FOR HEAT TRANSFER PROBLEM.....	26
HEAT AND MASS TRANSFER PRINCIPLES.....	27
Conduction.....	27
Convection.....	28
Radiation Heat Transfer.....	29
Radiation View Factors.....	31
Enclosure Theory.....	33
Solar Radiation.....	36
3. METHODOLOGY .....	37
RHINO3D MODEL.....	37
Bridge Models.....	37
Terrain Mesh.....	42
RADTHERM/RT THERMAL ANALYSIS SOFTWARE.....	42
GOVERNING EQUATIONS RADTHERM RT.....	45
Standard Elements.....	45
Three Layer Elements.....	50
Terrain Elements.....	50
Concrete and Asphalt Models.....	53
Foliage Models.....	56
Background Elements and Sky Elements.....	57
Element Definitions in RadThermRT.....	58

VIEW FACTOR CALCULATION IN RADTHERM/RT .....	59
View Factor Setting .....	59
View Factor Element Division Setting .....	60
Apparent Area Resolution View Factor Setting .....	61
Solution to Temperature Distribution .....	62
Experiment Method .....	63
DATA FORMATTING .....	66
Solar Data Formatting .....	67
Meteorological Data Formatting .....	70
INITIALIZATION .....	72
4. RESULTS AND FINDINGS .....	75
CONVERGENCE STUDY RESULTS .....	75
ADDITIONAL RESULTS .....	86
SHADOWING .....	88
LONGWAVE DATA .....	95
Instrumentation Issues .....	97
5. CONCLUSIONS AND RECOMMENDATIONS .....	99
REFERENCES .....	104
APPENDICES .....	108
APPENDIX A: WEATHER FILE DATA .....	109
APPENDIX B: MEASURED TEMPERATURE DATA .....	118
APPENDIX C: DATA FROM RADTHERM/RT SIMULATIONS .....	123

## LIST OF TABLES

Table	Page
1. Typical specific heats of concrete (partially reproduced from Table 6, Rhodes [1978]).....	23
2. Thermal conductivities of carbonate aggregate concrete. Reproduced from results [Rhodes1987],[Vodak et. Al,] [T.Z. Harwathy][H.Abe, et al 1970] .....	23
3. Shortwave radiation definitions (Touloukian and Dewitt[1972] and Plüss [1997]). .....	36
4. ITYPE for concrete and asphalt.....	53
5. Surface condition of pavement concrete nodes (ISURF) .....	53
6. Surface condition for asphalt nodes (ISURF).....	53
7. Moisture state IWET.....	53
8. Thermal properties for material groups. ....	54
9. Multiplying factor for capacitance and conductance. Adapted from ThermoAnalytics Terrain Model Technical Manual .....	55
10. Definition of Material Groups .....	55
11. Thickness definition for ITHK.....	56
12. View factor settings .....	61
13. Apparent area settings. Adapted from RadTherm manual.....	61
14. Variables for the .XWA, files adapted from RadTherm User manual.....	67
15. Correction factors supplied by Li-Cor for correcting diffuse readings taken with a shadow band. ....	69
16. View factor settings value.....	76

## LIST OF TABLES - CONTINUED

Table	Page
17. Calculation times for view factors(VFC) and solution calculation (SC) times for twelve hour simulations run on Silicon Graphics Origin 2100 Server.....	79
18. Nighttime simulation statistics for April 7, 9:00pm through April 8, 8:55am with low view factor settings and varying element size. ....	82
19. Nighttime simulation statistics for April 7, 9:00pm through April 8, 8:55am with default view factor settings and varying element size. ....	82
20. Nighttime simulation statistics for April 7, 9:00pm through April 8, 8:55am with high view factor settings and varying element size. ....	82
21. Daytime simulation statistics for April 8, 9:01 am through April 8, 8:46 pm with low view factor settings and varying element size. ....	83
22. Daytime simulation statistics for April 8, 9:01 am through April 8, 8:46 pm with default view factor settings and varying element size. ....	83
23. Daytime simulation statistics for April 8, 9:01 am through April 8, 8:46 pm with high view factor settings and varying element size. ....	83
24. Summary of results for simulations; March 13, 6:50 am to March 13, 6:45pm, April 7, 9:00 pm to April 8 8:55 am, April 8, 9:01 am to April ,8 8:46 pm, April 8, 9:01 pm to April 9, 1:36 am with default view factors and 3000 elements bridge mesh .....	86

## LIST OF FIGURES

Figure	Page
1. Bozeman pass RadTherm/RT thermal model.....	8
2. Meridian surface temperature and wind forecast of I-90 Corridor.....	13
3. Coastal Environmental meteorological station.....	16
4. Radiation instruments including two Li-Cor pyranometer and one Epply PIR.....	17
5. LI-200SA spectral response curve. Copied from LI-COR Terrestrial Radiation Sensors [1986] with permission.....	18
6. Omega IR thermometer.....	20
7. Spectrum of electromagnetic radiation highlighting thermal region (values from Incropera and Dewitt [1996]).....	30
8. Geometry for exchange between finite areas (adapted from Siegel and Howell [1992]).....	32
9. Example enclosure with N surfaces.....	33
10. Radiative terms on surface area A.....	35
11. Perspective view of terrain mesh.....	38
12. Top view of bridge meshes, (A) is the 10 elements bridge mesh, (B) is the 300 elements bridge mesh and (C) is the 3000 elements bridge mesh.....	38
13. Example of a Rhino3D polyline with several vertices.....	39
14. Steps in creation of 3000 elements bridge mesh , (A) bridge outline is drawn using polylines, (B) polylines are drawn where supports will be, (C). polylines drawn around outline of supports and barriers, (D). close up of mesh showing aligned vertices, (E) perspective of 3000 elements bridge mesh.....	40

## LIST OF FIGURES - CONTINUED

Figure	Page
15. Cross section view showing simplification made on supports and barriers, (A) is from bridge blue prints and (B) is the cross section of modeled bridge. ....	41
16. Polygon mesh detailed options from Rhino3D.....	42
17. Standard element.....	46
18. Heat transfer modes into standard element.....	46
19. Three layer elements.....	50
20. Terrain elements.....	52
21. Schematic representing foliage nodes. (taken from ThermoAnalytics website).....	57
22. Terrain element definitions, (A) elements defined as Interstate Asphalt, (B) elements defined as county road asphalt, (C) elements defined as heavy concrete pads, (D) elements defined as short grass foliage. ....	58
23. View factor calculation. (1) two meshes view each other, (2) a hemisphere is constructed in each element and rays are cast intersecting other elements, (3) showing all of the rays cast from a single element. Graphics from ThermoAnalytics website.....	60
24. WTI mobile lab with WeatherPak meteorological station deployed.....	65
25. Example of a portion of an extended weather format file. ....	68
26. Description of data formatting method steps 1-4.....	73
27. Description of data formatting method steps 5-7.....	74
28. Temperature comparison between measured temperature and calculated temperature for daytime simulations run on data from April 8 9:01 am to April 8 8:46 pm with Default view factor settings; (A) results from the 3000 elements bridge mesh, (B) results from the 300 elements bridge mesh and (C) results from the 10 elements bridge mesh.....	78

## LIST OF FIGURES - CONTINUED

Figure	Page
29. Correlation graph for 300 elements bridge mesh with high view factor settings April 8, 9:01 am through April 8, 8:46 pm. ....	84
30. Correlation graph for 3000 elements bridge mesh with high view factors from April 8, 9:01 am through April 8, 8:46 pm data. ....	84
31. Histogram graph of 300 elements bridge mesh data with high view factors from April 8, 9:01 am through April 8, 8:46 pm data and associated normal curve distribution. ....	85
32. Histogram graph of 3000 elements bridge mesh data with high view factors from April 8, 9:01 am through April 8, 8:46 pm and associated normal curve distribution. ....	85
33. Temperature comparison between measured temperature and calculated temperature for March 13, 2003 with standard view factor settings. ....	87
34. Temperature comparison between measured temperature and calculated temperature for March 8-9 with standard view factor setting. ....	87
35. Shadowing on terrain below bridge with bridge hidden from view. ....	91
36. Shadowing on section of large element number mesh bridge. ....	92
37. Temperature values for three elements lying in pedestrian walkway from east to west. For large number of bridge elements bridge mesh from April 8 daytime simulation. ....	93
38. Solar flux values from April 8 daytime simulation indicating times when values undergo rapid change due to variable shadowing conditions. ....	93
39. Temperature values for element lying in pedestrian walkway for 300 elements bridge mesh from April 8 daytime simulation. ....	94
40. Layout of bridge geometry showing element edges and area of bridge measurement. ....	94
41. March 13 simulation with offset bad longwave data. ....	97

LIST OF FIGURES - CONTINUED

Figure	Page
42. March 13 simulation with Bozeman Pass RWIS longwave data.....	97

## NOMENCLATURE

A	Area ( $m^2$ )
$AA_k$	Apparent area that the radiation sees ( $m^2$ )
$A_k$	Surface area exposed to convection ( $m^2$ )
C	Correction factor from Table 15
c	Speed of light (m/s)
$c_p$	Specific heat (J/kg-K).
$c_p$	Specific heat of the body (J/kg-K).
$C_{rc}$	Specific heat reinforced concrete (J/kg-K).
$D_c$	Corrected diffuse radiation ( $W/m^2$ )
$D_L$	Measured value of diffuse solar radiation ( $W/m^2$ )
$E_b$	Emitted radiation (Watts)
$E_r$	Rate that the real surface emits radiant energy (Watts)
$F_{j-k}$	View factor of area $A_j$ that arrives at area $A_k$
G	Measured global solar radiation value ( $W/m^2$ )
h	Convection heat transfer coefficient ( $W/m^2-K$ )
$h_k$	Convection coefficient ( $W/m^2-K$ )
k	Thermal conductivity ( $W/m-K$ )
$k_{kj}$	Thermal conductivity of the material between thermal nodes j and k ( $W/m-K$ )
L	Length (m)
$L_{kj}$	Geometric distance between node k and node j (m)
m	Mass of the body (kg)
$m_k$	Mass of element k (kg)
N	Total number of surfaces
$N_{cond}$	Total number of conduction links between node k and all adjacent nodes
Q	Net heat transfer rate (Watts)
$Q_c$	Heat transfer rate carbonate concrete (Watts)
$Q_{con}$	Conduction heat transfer rate (Watts)
$Q_{conv}$	Convection heat transfer rate (Watts)
$Q_{DiffR}$	Global diffuse radiation (Watts)
$Q_{DirR}$	Direct solar radiation (Watts)

$Q_{GR}$	Total global radiation (Watts) Incident radiant energy from other elements in the enclosure
$q_{i,k}$	( $W/m^2$ )
$Q_j$	Outgoing radiation (Watts)
$Q_k$	Heat transfer rate from the surface or as the net radiative loss from the surface to the enclosure (Watts)
$Q_{lw}$	Longwave radiation flux of the sky in Watts
$Q_{mass,k}$	Defined for each different terrain application type (Watts) Explicit heat transfer rate imposed by the short wave solar energy
$Q_{netS}$	(Watts)
$Q_{netSk}$	Explicit term involving the amount of solar radiation node k is receiving (Watts)
$q_{o,j}$	Outgoing radiative terms from the other areas ( $W/m^2$ )
$q_{o,k}$	Emitted plus the reflected radiant energy ( $W/m^2$ )
$Q_{rad}$	Radiation heat transfer rate (Watts)
$Q_{radk}$	Net radiative loss from surface k (Watts)
$Q_{rc}$	Heat transfer rate reinforced concrete (Watts)
$Q_{ref\_in,k}$	Amount of solar radiation reflected into element k from all other elements and the default background element (Watts)
$Q_{ref\_out,k}$	Amount of solar radiation reflected out from node k (Watts)
$Q_s$	Heat transfer rate reinforced steel (Watts)
$Q_s$	Total amount of solar radiation received including direct and diffuse solar radiation (Watts)
$Q_{solar,k}$	Amount of solar radiation into node k (Watts)
$Q_T$	Net rate of radiation from the smaller surface (Watts)
$Q_x$	Heat rate by conduction through a plane wall of area A (Watts)
S	Length (m)
t	Independent variable time (seconds)
$T_{\infty}$	Bulk temperature of the fluid (Kelvin)
$T_f$	The temperature of the fluid that is convecting heat to or away from $A_k$ (Kelvin)
$T_s$	Temperature of the surface (Kelvin)
$T_{sur}$	Surface that surrounds the smaller surface (Kelvin)
$VF_k$	Visibility factor used for shadowing
$\dot{w}$	Rate of work done (Watts)

x	RadTherm modeled values (Kelvin)
y	Actual temperature data (Kelvin)
y(t)	Dependent variable
$\alpha$	Absorptivity
$\alpha_k$	Absorptivity of node k
$\alpha_{td}$	Thermal diffusivity ( $m^2/s$ )
$\Delta T$	Change in temperature (Kelvin)
$\delta_{kj}$	Kronecker delta defined $\delta_{kj} = \begin{cases} 1 & \text{When } k = j \\ 0 & \text{When } k \neq j \end{cases}$
$\varepsilon$	Emissivity
$\theta_j$	Angle j
$\lambda$	Spectrum of wavelengths $\mu m$
$\mu_x$	Mean value of all of the modeled temperature readings (Kelvin)
$\mu_y$	Mean of the measured temperature (Kelvin)
$\nu$	Frequency
$\rho$	Density of the material ( $kg/m^3$ )
$\rho_c$	Density concrete ( $kg/m^3$ )
$\rho_r$	Reflectance
$\rho_s$	$A_k$ density steel ( $kg/m^3$ )
$\sigma$	Stefan-Boltzmann constant $5.67 \times 10^{-8} (W/m^2 \cdot K^4)$

## ABSTRACT

A model was developed to calculate the time varying temperature of a highway overpass bridge. This model geometry was drawn using a three-dimensional CAD program, which was also used to discretize the model's geometry into a mesh. This meshed geometry was then imported into RadTherm/RT for thermal analysis. RadTherm/RT is a multi-mode finite differencing heat transfer code. Conduction, wind convection, solar radiation which can account for shadowing and long wave radiation are the heat transfer modes accounted for by the software. The meshed geometry had material properties assigned to it, including; density, specific heat and thermal conductivity. In addition surface properties were applied, including; emissivity and absorptivity. Emissivity is a measure of how well a body emits thermal radiation and absorptivity is a measure of how well a body absorbs thermal radiation. In addition an instrumentation and data acquisition system were developed for measuring model inputs. Model inputs measured were; air temp (deg C), wind speed (m/s), wind direction (deg), barometric pressure (mmhg), relative humidity (%), total global solar radiation flux ( $W/m^2$ ), diffuse solar radiation ( $W/m^2$ ) and sky temperature (deg C). These values were measured over extended time periods, with five minute time steps. These inputs were then formatted for input into RadTherm/RT. In addition to these parameters a single non-contact surface temperature was measured on the bridge deck (deg C) for use in comparing to the computer solution. A convergence study was also performed to analyze how mesh size and settings in RadTherm/RT affect the accuracy of the solution. Two parameters were varied; the size of the elements used in the bridge mesh and a setting used in the program for calculation of view factors. Results of the convergence study reinforce the idea that the accuracy does increase with increasing the number of elements and increasing the view factor settings. The overall accuracy of the model was found to be adequate to justify further study and development of model. The overall conclusion is that the model is accurate in modeling the time varying surface temperature conditions that a bridge deck experiences.

## INTRODUCTION

Winter highway travel impacts the lives of everyone who lives in an area that experiences road icing events. Icing on roads can present dangerous driving conditions, which increase the rate of accidents, and slow down the transport of goods. This has wide reaching economic costs. During the past ten years there have been advances in winter highway maintenance in ice prevention on roadways. These methods require advance warning of roadway temperatures that are approaching the freezing point of water. Maintenance managers need time to plan and prepare for icing events. A system that can help to predict the surface temperature of roadway surfaces requires multi-mode heat transfer analysis. This coupled system of conduction, convection, and radiation heat transfer, requires a numerical method of solution. The radiative portion plays a major role in the surface temperature of roadways.

A model that can predict surface temperatures while accounting for all forms of radiation, would be an advance on current road temperature forecasting, which focus on metrological factors, and often do not adequately account for radiation modes of heat transfer [Ballard et al 2002]. In this thesis the thermal modeling software, RadTherm/RT (Radiation based Thermal model for Road Temperature), is used to calculate the surface temperature of a highway overpass bridge, and the neighboring roadways and terrain. To evaluate the performance of the software, this evaluation was carried out by measuring the data inputs to the model and concurrently measuring the surface temperatures of the bridge deck at a single point. Twelve to thirty six hour data collection periods were carried out on, a highway overpass bridge. Input to the model includes meteorological

data and solar radiation parameters including; long-wave radiation, short-wave solar radiation, and diffuse solar radiation.

Winter highway maintenance is primarily the responsibility of state and municipality Departments of Transportation (DOT). Montana's Maintenance provider is the Montana Department Of Transportation, MDT. Among their winter maintenance tasks are plowing roads and applying chemicals and abrasives to roads. In order to efficiently use resources, they maintain extensive information, communication, and weather monitoring systems.

A common procedure of traditional snow and ice control practice is to wait until an inch or more of snow accumulates on the pavement before beginning to plow and treat the highway with chemicals or abrasives [Boselly 2001]. While this procedure is straightforward, it frequently leads to a compacted snow layer (pack) that is tightly bonded to the pavement surface. A subsequent "deicing" of the pavement is then necessary, usually requiring a large quantity of deicing chemicals, and abrasives to work their way through the pack to reach the snow/pavement interface and destroy or weaken the bond [Ketcham et al 1996]. The abrasive is often mixed with a solution of deicing chemicals. These chemicals help the sand to penetrate into the compressed snow or ice on the roadbed. The most commonly used deicing chemical is sodium chloride [Gray- Fisher 2000]. One of the major problems of waiting until after precipitation has already fallen, is the strong bond that can form between the road and the precipitation. Boselly [2001] reports that after a bond has formed it takes five times more energy to remove the snow or ice from the road surface. If the bond could be prevented from forming then the snow

or ice could be removed more efficiently and fewer chemicals would be required. Once the bond has formed a large amount of chemical deicers must be used to break down this bond. A standard application rate of salt for deicing is around 300 lbs per lane mile [Ketcham et al 1996]. Among the environmental and economic impacts of highway salt usage are, poisoning roadside vegetation, increasing concentrations in adjacent waterways, and corrosion to vehicles [Ketcham et al 1996]. There are also some air quality concerns with the use of abrasives; cities that struggle with EPA regulations on clean air standards often ban the use of abrasives [Nixon 2001]. The abrasives are ground up when driven over and increase the amount of particulates in the air. A method that prevents the bonding of ice to pavement can reduce the amount of chemicals used and remove the need for applications of abrasives, providing for a more efficient method for removal of snow/ice.

Anti-icing is a strategy in winter highway maintenance that has been growing in support for the last decade [Boselly 2001]. Anti-icing is the snow and ice control practice of preventing the formation or development of bonds between precipitation and the road surface, by timely application of chemical freezing-point depressants. It involves maintenance crews getting out before or during the onset of a winter storm to apply liquid brine to the surface of the roads that could have ice formation. The most common chemical in use today in anti-icing is magnesium chloride [Gray-Fisher 2000]. This brine mixes with the snow/ice at the surface of the road effectively lowering the freezing point of the mixture, decreasing bond formation and strength. This method has been shown to greatly reduce the amount of ice on roadways during and after a storm [Boselly 2001]. It

also makes removing the precipitation easier since it does not form a solid surface on the roadbed. Anti-icing uses between 75 and 250 lbs per lane mile of chemicals depending on the amount of precipitation expected [Ketcham et al 1996]. An effective anti icing program requires the use of a systematic approach to snow and ice control. This approach will maintain roads in the best conditions possible during a winter storm, while minimizing chemical usage. As a consequence, anti-icing has the potential to provide the benefit of increased traffic safety at the lowest cost. However, to achieve this benefit the maintenance manager must adopt a systematic approach to snow and ice control to ensure that the performance of the operations is consistent with the objective of weakening the formation or development of the bond between the precipitation and the road[Nixon, 2002]. To optimize efficiency this method also requires site-specific weather forecasting, including some prediction of road surface temperatures. Consequently accurate thermal mapping of road surfaces can be a huge benefit. The road surface temperature is important for two reasons. If the road surface is not below freezing no ice will form, so no chemicals need to be applied, and if the road is too cold, where the mixture of chemicals and precipitation on the road would be below the eutectic temperature of the mixture then anti-icing is ineffective.

Maintenance managers are responsible for the scheduling of maintenance tasks. Thus they need to know that a storm is coming, when it is going to start, expected precipitation amounts, and types of precipitation. They need to make sure that they have all of the materials that will be needed in a storm. It is important to know when the storm is starting so that the chemicals are not applied too early; this insures that there is an

adequate amount of chemicals on the road when the precipitation starts, and when the road temperature is below the freezing point. The amount of precipitation is important in deciding the rate of chemical application needed to insure that the freezing point of the precipitation is depressed enough to prevent icing, it may also be necessary to reapply chemicals during the storm.

A tool that has been identified as vital to a successful anti icing program is Remote Weather Information System, (RWIS) stations. RWIS stations are strategically located near critical road sections, such as mountain passes or bridge decks. RWIS stations contain data collection and communication systems and data delivery systems. Typical data collections system monitor; air temperature, relative humidity, wind speed, wind direction and precipitation. They generally have embedded pavement sensors that measure road surface and subsurface temperatures. These embedded sensors often also monitor the freezing point and chemical concentrations. However these sensors only give data at a single point on the road. Pavement temperature has high spatial variability. These sites can also be outfitted with cameras and solar instruments, several state DOT's have stated that they would like to have solar pyranometers included into their systems [Ballard et al 2002].

RWIS sites are estimated to cost between \$50,000 to \$75,000 to purchase and install, and up to \$2,000 per year in maintenance costs [Nixon, Personal communication]. Location of each installation must be carefully analyzed. Also there are finite number of sites that can be feasibly installed and maintained. Montana currently maintains 59 sites, and has recently identified six potential new locations.

RWIS stations are also used in developing road weather forecasts. They are used to help define the boundary conditions of the forecasts and can be a useful tool for comparing what the forecast predicts and what is actually happening at a specific location. These forecasts are generally for specific areas of interest and are called site-specific forecasts. Data from the stations are also used to help create forecast surface temperature maps.

This forecasting is necessary as the RWIS sites only provide weather information at exact locations and a means of interpolating data between sites is necessary. A private meteorology firm based in South Dakota provides road weather forecasts for MDT. Their forecasts are based on national weather satellite data, weather models from the National Center for Environmental Prediction (NCEP) and RWIS data. This data is collected and used as input into meteorological forecast software called Advanced Regional Prediction System, or ARPS. ARPS was developed at the University of Oklahoma's Center for Analysis and Prediction of Storms, CAPS. CAPS mission is to "demonstrate the practicability of storm-scale numerical weather prediction and to develop, test and validate a regional forecast system"[Xue, et al, 2001]. The software that came out of this program is ARPS, with the first version appearing in 1994 and the latest version appearing in 2001. Using ARPS weather forecasts are produced on refined grids with adjustable time scales. ARPS can also produce surface temperature maps of the same resolution as the meteorological forecasts. These refined forecast are then distributed to the necessary divisions of MDT. Utah DOT decided to discontinue the purchasing of surface temperature maps due to the fact that they generally only predicted the daily

freeze thaw cycle and were not useful for maintenance decisions [Ballard 2001]. Some of the negative aspects associated with the surface temperature maps will be discussed in greater detail in the next chapter. A software program has been developed that can more accurately predict road surface temperatures using the same ARPS meteorological forecast data. RadTherm/RT is a thermal modeling program derived from earlier codes that were originally created for the military in identifying and modeling thermal signatures of vehicles. RadTherm/RT has been developed to solve multi-mode heat transfer utilizing advanced radiation solvers. The governing equations to the heat transfer problem are solved using the Crank-Nicolson Method, this method utilizes a central differencing scheme for both the time and space variable. This implicit method requires the solving of a set of simultaneous equations at every time step. The software produces a thermal map of calculated surface temperatures, with adjustable time steps between the calculated temperatures. The temperatures of nodes that do not lie on the outer surfaces are also calculated, and can be exported for use in spreadsheet programs.

A weather modeling chain culminating with a RadTherm/RT model of Bozeman Pass between Bozeman and Livingston has been created, and is running in a forecast mode that updates a website to display the road temperatures graphically. This model uses a mesh with a 30 meter resolution, and is shown in Figure 1. Presently there are no structures or bridges incorporated into the model. It would be useful to incorporate bridges into the model because the temperature on the bridge deck is often significantly different than the neighboring roadway. As most drivers know highway bridges are more likely to freeze and freeze more quickly than the rest of the highway. This is due to the

fact the roadway receives heat from the ground by conduction and only has convection and radiation losses on one surface. Bridges have less thermal mass and have convection and radiation losses on two surfaces. This surface freezing on bridge decks can be dangerous to the driving public because the condition of the road surface may change from wet on the roadway to black ice on the bridge. Thus maintenance crews may have to apply anti-icing chemicals to the bridge deck earlier and possibly more often than to the pavement in order to maintain a satisfactory level of service. The ability to predict freezing on bridge decks could allow for more efficient use of anti-icing chemicals and the ability to maintain the acceptable condition of the bridge deck.

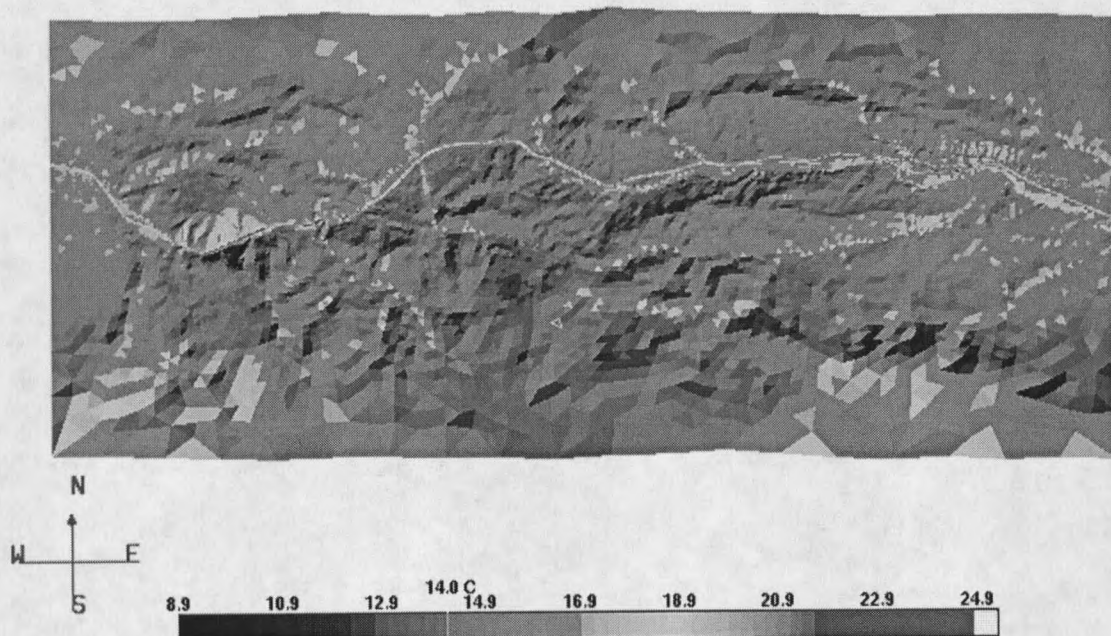


Figure 1. Bozeman pass RadTherm/RT thermal model.

In this thesis first principle thermal models are used to predict possible icing condition on a highway bridge. RadTherm/RT is used to analyze the model and the 19<sup>th</sup> Street Bridge over I-90 in Bozeman, MT is used as an example. The solution to the surface temperatures is the simultaneous solution to multi-mode heat transfer equations. It is very difficult to derive an analytical solution to these types of problems so a numerical method is employed [Siegel Howell 1991]. RadTherm/RT uses a spatially implicit finite difference forward time stepping scheme to solve for the surface temperatures. Each element in RadTherm/RT requires a definition to be applied, the Bozeman pass RadTherm/RT model used terrain elements exclusively. Terrain elements have thermal nodes that are coupled to a subsurface node that is below ground to a depth where the temperature is diurnally stable, and which is generally known. This subsurface temperature is used as a boundary condition to help solve for the surface temperature. The terrain elements allow the user to specify whether the terrain is a road surface, rocky surface, vegetative surface, water or snow. Each of these types of terrain has some adjustable parameters that can be set by the user. In the model used in this thesis only the area around the bridge was modeled with terrain elements, The bridge structure was represented with standard and three layer elements.

These elements are more general than the terrain elements and require more parameter definitions than do the terrain elements. The bridge deck was modeled with an exposed lower surface. Thus in the model there is convection on the top and lower surfaces, conduction internally and between the support structures of the bridge and the bridge deck itself, radiation between surfaces and imposed solar radiation loading. In

addition to the solar loading there are also shadowing effects on the bridge due to the concrete barriers on the bridge deck and on the terrain under the bridge.

The conduction through the bridge deck and between the bridge deck and support structures is dependent on the thermal conductivity. The thermal conductivity is dependent on the materials used in constructing the bridge deck. Average values are slightly higher than those of concrete due to the steel reinforcement. It is assumed in the analysis that the material is homogenous and isotropic with respect to thermal conductivity.

Convection takes place at the exposed surfaces of the bridge. RadTherm has three options for calculating the convection coefficient for standard elements. The magnitude of this mode of heat transfer is largely dependent on the wind velocity and the air temperature compared to the bridge temp.

The radiation heat transfer is imposed in two major ways. There is the radiation between two surfaces that "view" each other, and there is the solar radiation from the sun. The magnitude of the first type of radiation is the difference between the two surface temperatures taken to the fourth order. This mode also is dependent on some optical surface properties, mainly surface emissivity. Emissivity is unity for a black body and for real surfaces is a fraction that depends upon temperature and surface parameters: roughness, texture, color, material, and coatings [White, 1991]. For this thesis it is assumed that all radiation surface properties including emissivity, and absorptivity values are averaged over temperature and angle. This is a gray body assumption, thus all bodies in analysis are considered gray bodies. The other mode of radiation heat transfer is

explicitly solved for using measured or forecast data. This includes direct solar radiation, diffuse solar radiation and reflected portions of solar radiation [Temps et al. 1977]. In calculating the solar loading, RadTherm/RT also accounts for shadowing effects.

It is desirable to have a model that can accurately predict the surface temperature of the bridge deck, using weather and selected wavelengths of solar radiation data as the input. The inputs for the model presented here were measured using a mobile weather station and include; air temperature, wind speed, wind direction, relative humidity and barometric pressure. In addition, three solar radiation instruments were used to measure the total global solar radiation, global solar diffuse radiation, and long wave radiation. An infrared handheld thermometer was used to measure the actual surface temperature of the bridge. The data from this instrument was compared with output from the model. Once established that the RadTherm/RT bridge model can accurately calculate the surface temperatures using measured weather data, this model may then be applied using meteorological forecasts. A RadTherm/RT model that can accurately forecast roadway temperatures and bridge deck temperatures would be a great tool for DOT maintenance managers. It would allow them to anticipate an icing event. In essence, these forecasts could help to improve the level of service to roads and ensure safer driving conditions.

## BACKGROUND

### Current Thermal Mapping

Most DOTs use a private contractor for their meteorological forecasting. Although these may include surface temperature forecasts they are not road specific forecasts. MDT contracts with a North Dakota firm, Meridian. This company issues meteorological forecast typically every twelve hours. They collect meteorological data from a variety of sources, including the National Center for Environmental Prediction (NCEP). weather data from RWIS sites, and from other sources such as airports that publish meteorological data. NCEP runs a large scale weather forecast, ETA, that is broken up into geographical regions in 20 km grids. The ETA data is distributed in three-hour time steps, thus any atmospheric features that are small enough to traverse from outside the boundaries of the domain to inside the domain in less than three hours would be ignored. Meridian downloads the data for the Pacific Northwest Region and they run a nest model with 20 km resolution, using a meso scale meteorological forecast program called, Advanced Regional Prediction System (ARPS). ARPS provides a run that has higher resolution in time, and includes some atmospheric features that may have been ignored by the ETA model. In addition ARPS utilizes Digital Elevation Maps to increase the accuracy of their forecast. The forecasters at Meridian also consult the RWIS data for modifying the boundary conditions. Then using data from the 20 km resolution ARPS model a finer nested resolution (3km) model is run for areas of interest to the DOTs. This forecast is then used to create thermal maps. All of this information is then passed to the DOTs for

maintenance planning [conversation with John Mewes, 2002]. These thermal maps are meteorological based and often provide good forecasts for air temperature, relative humidity and other meteorological data, but less satisfactory results for surface temperature forecasts. They generally do not consider shadowing effects, have limited knowledge of surface albedo and do not distinguish between a road surface and the surrounding terrain. Thus in mountainous regions these maps can be highly inaccurate. Figure 2 shows an example of a Meridian produced surface temperature forecast map of Bozeman Pass using a 3km resolution grid.

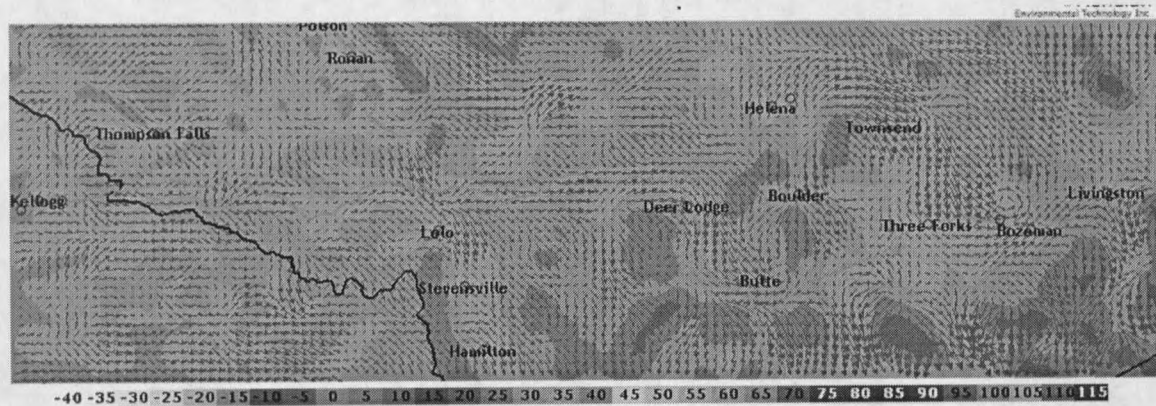


Figure 2. Meridian surface temperature and wind forecast of I-90 Corridor.

### RadTherm/RT

The genesis of the RadTherm/RT software is based on two computational models utilized by the U.S. military for prediction of vehicle infrared signatures. The first principle heat transfer software from which the pavement model was derived is the TCM (Thermal Contrast Model), developed for the U.S. Air Force [Johnson, K.R, 1991,

Johnson, K.R., et al, 1996], also used is PRISM (Physically Reasonable Infrared Signature Model) developed at Michigan Technological University's Keweenaw Research Center in partnership with the U.S Army Tank-automotive Command (TACOM)[Prism 3.0 user's Manual, 1991].

The purpose of these programs was to model the surface temperature of the vehicles to be used in infrared imagery simulations. The surface temperatures of a vehicle subject to a set of meteorological conditions gives a specific thermal signature. To simulate these signatures, the 3-D geometry of the vehicles was defined by a series of flat plates or facets. Originally the background was modeled as an isothermal flat plate. A topographically varied terrain model was developed for snow by, Adams and McDowell[1991], as background. This was extended to other backgrounds. Subsequent availability of Geographic Information Systems (GIS) along with availability of Digital Elevation Maps (DEM) offered digital sources for complex background models. GIS data was used to obtain information about the properties of the terrain; this information along with DEM data can now be readily input into a RadTherm model. This method of utilizing DEMs and GIS was developed in the MPART program. Currently RadTherm/RT is being used in the Greater Yellowstone Regional Traveler and Weather Information Systems Project (GYRTWIS). One of the tasks in this project is modeling the Interstate highway, and surrounding terrain between Livingston Montana and Lookout pass on the border of Montana and Idaho. The goal of the project is to generate reasonably accurate forecasts of the road surface temperature. This knowledge could be

of great help in applying anti-icing principles, and increasing traveler awareness for this stretch of highway.

By including detailed terrain features, RadTherm/RT is potentially much more accurate for forecasting road surface temperatures than models that only utilize meteorological data. The output is a three dimensional thermal map and clearly shows regions that have temperatures of interest. Its ability to calculate shadowing along with its advanced radiation solvers could make it a much more useful tool to maintenance managers than previously available surface temperature maps developed by meteorologists. The GYRTWIS Bozeman pass project is using the weather forecast from Meridian as the data input and computes road temperature forecasts twice daily and automatically updates a website with graphical representations of the forecast road temperatures.

#### Instrumentation

In addition to a standard meteorological package used from Coastal Environmental Systems, three radiation sensors were utilized. Two Li-Cor pyranometers were utilized and one Epply Precision Infrared Radiometer (PIR). The Li-Cor pyranometers measure the solar spectrum between 0.4 to 1.2  $\mu\text{m}$ . The PIR is sensitive to the electromagnetic spectrum between 3.5 to 50  $\mu\text{m}$ . All of these instruments were specified and purchased for use in model validations. A great deal of time went into developing this instrumentation package and making all of the different instruments work properly. In addition a data acquisition system had to be developed for these instruments.

Coastal Environmental WEATHERPAK.

The WEATHERPAK meteorological station instrument package measures; wind speed and direction, air temperature, relative humidity and barometric pressure. All of the instruments are sealed in the body of the instrument and all data is stored locally in the system which communicates with proprietary software, INTERCEPT™, to collect, display, archive and share data. The instrument is shown in Figure 3.

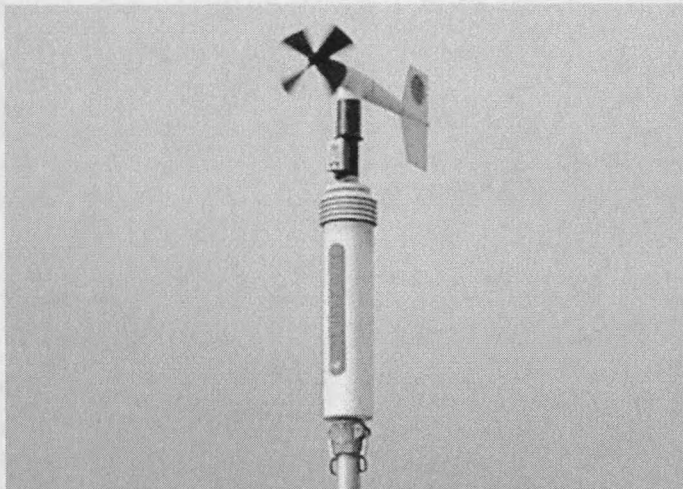


Figure 3. Coastal Environmental meteorological station.

Licor pyranometer.

The LI-COR 200SA pyranometer sensor is a field ready global solar radiation sensor. It is used for measuring short wave solar radiation and is sensitive to wavelengths between 0.4 to 11.2  $\mu\text{m}$ . It measures global solar radiation and if the direct solar beam is blocked can be used to measure global diffuse radiation. For this project, it was used in a level position to measure incoming solar radiation, this is shown in Figure 4. The current

output of the sensor is directly proportional to solar radiation. The response of the photodiode used in this sensor is not ideal for the relative spectral response for this sensor. An ideal response would be an equal reaction over the entire short-wave spectrum of .280-2.80  $\mu\text{m}$ . The typical response curve of the pyranometer is shown in Figure 5. This response is very weak at 0.4  $\mu\text{m}$  increasing almost linearly to a maximum sensitivity at 0.95  $\mu\text{m}$  and then linearly decreasing until a cutoff close to 1.2  $\mu\text{m}$ . However the absolute error when compared to the highest precision instrument is  $\pm 5\%$  maximum, typically  $\pm 3\%$ . [Licor Manual]. The LI-200 is factory calibrated against an Epply Precision Spectral Pyranometer.

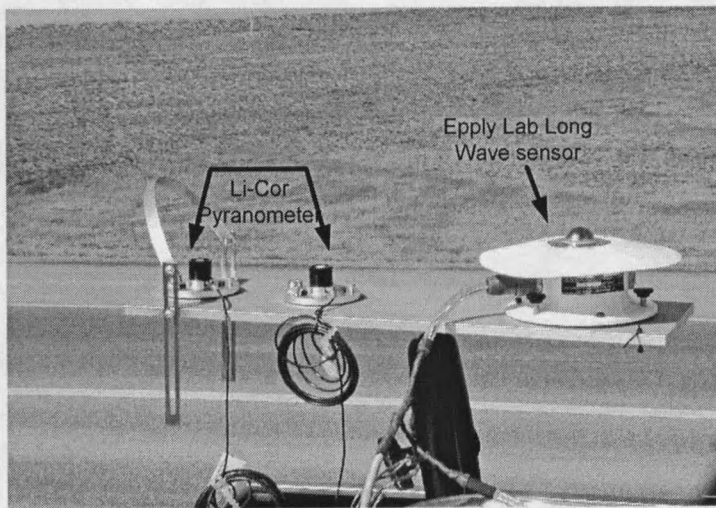


Figure 4. Radiation instruments including two Li-Cor pyranometer and one Epply PIR.

The Li-200SA can be converted to output millivolts with a 147-ohm adapter. This adapter was used for both sensors to ease data acquisition. A mounting and leveling

fixture was also purchased for the sensors. This was used to mount to the plate that holds all of the sensors.

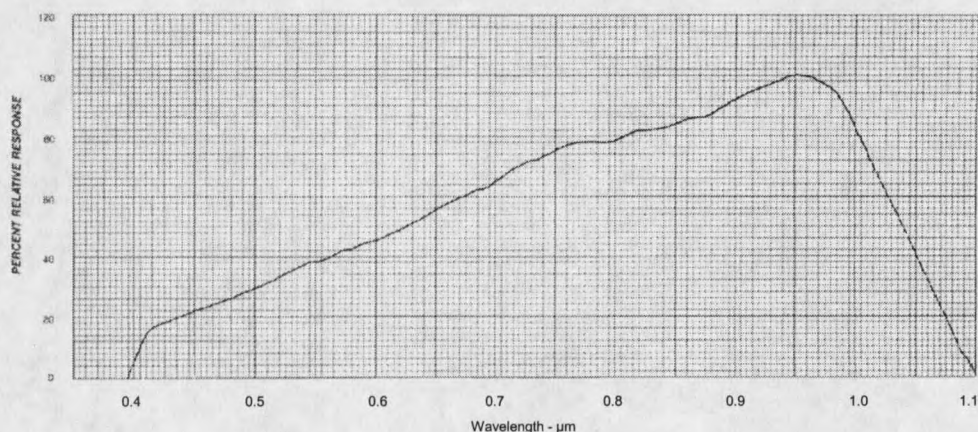


Figure 5. LI-200SA spectral response curve. Copied from LI-COR Terrestrial Radiation Sensors [1986] with permission.

The second Pyranometer was used to measure diffuse solar radiation. Fitting a shadow band to block the direct solar beam from the sun allows this measurement to be taken, see Figure 4. A shadow ring that just blocked the direct solar beam and nothing else would be beneficial, however it would have to be moved every few minutes to assure that the sensor was still in the shade. This shadow band was manufactured for this project using the specifications of a product that Li-Cor discontinued several years ago. The band is six inches in diameter and a half inch thick. The shadow band, once aligned keeps the sensor shaded for a day or two, requiring for minimal adjustment during the testing periods. The amount of sky that is blocked, which does not include the direct solar beam, is accounted for by using a calibration table supplied by LI-COR. It gives a correction factor determined by the latitude and the month of the year, and is used to correct the

amount of diffuse radiation measured. In RadTherm the direct solar radiation can then be computed from the relation,

$$Q_{GR} = Q_{DiffR} + Q_{DirR} \quad (1)$$

Where  $Q_{GR}$  is the total global radiation and  $Q_{DiffR}$  is the global diffuse radiation and  $Q_{DirR}$  is the direct solar radiation. Thus the  $Q_{GR}$  and  $Q_{DiffR}$  are measured and the  $Q_{DirR}$  can be easily calculated.

#### Epply PIR.

The long wave infrared sensor was purchased from The Epply Laboratory, Inc. (Fig X.) It is a precision Infrared Radiometer. It is designed to measure global long-wave radiation. The sensor has a filtered dome, this filter blocks the short-wave radiation and allows the transmittance of long wave radiation. "Tests have demonstrated that this filter does not exhibit significant transmission of short wavelength radiation" [Epply lab PIR instruction sheet]. The transmission envelope has a sharp transition between 3 and 5  $\mu\text{m}$ , from complete opaqueness to maximum transmittance for the long wave radiation, and a transmittance range of 3.5 to 50  $\mu\text{m}$ . This dome also protects the sensor from the outside elements. The actual sensor is a circular multi-junction wire-wound Eppley thermopile. Its receiver is coated with Parson's black lacquer, a wavelength independent absorption material. See Figure 4 for a picture of the sensor. A thermistor is installed inside of the dome and measures the temperature of the dome, which is used in a temperature compensation circuit. A thermistor battery resistance circuit is used to accurately compensate for emitted radiation. The instrument outputs a voltage that is proportional to

the received long wave radiation. To obtain the radiation measurements in units of  $W/m^2$ , the output voltage was divided by the sensitivity of the instrument. The sensitivity for the instrument used in fieldwork was  $4.31 \times 10^{-6} V/W \cdot m^{-2}$ . Calibration is traceable to the International Practical Temperature Scale (IPTS). Some trouble was encountered in using this specific device. Much of the data used was from a PIR mounted at the Bozeman pass RWIS station. The reasons behind the use of the data from the pass is discussed in detail in chapter four.

#### Handheld Infrared Thermometer.

The handheld infrared thermometer used is an Omega OS521 surface temperature measurement device. (Fig 6.) This thermometer has adjustable emissivity from .1 to 1 with tenth increments. It has a response rate of 250 microseconds. A 1 milli-volt per degree analog output that can be interfaced with data acquisition equipment. The field of view ratio is 20:1 (e.g at a distance of 20 cm it will focus on an area that is 1 cm in diameter). The thermometer is shown in Figure 6.



Figure 6. Omega IR thermometer.

### Material Properties.

A large set of material properties may be assigned to elements in RadTherm. For terrain elements, RadTherm uses internally defined values for each terrain type. New terrain definitions may be added at the software programming level. In addition to the terrain elements are more general elements which require material property definitions to be assigned. The material properties that are assigned to standard and three layer elements include; specific heat, thermal conductivity and density.

#### Specific Heat

Specific heat is defined as the amount of energy required to raise a unit mass of material 1 degree. In SI units specific heat is expressed in J/kg K. The different types of aggregates typically used in concrete have little effect on the specific heat of concrete [Rhodes, 1978]. Some measured values of specific heat of concrete are listed in Table 1. The specific heat is however affected by the presence of steel reinforcement in the bridge deck [Lie et al., 1995], typically should resulting in a slightly higher value. An equation proposed by Lie and Kodur [1995] for the calculation of specific heat,  $C_{rc}$  (J/kg K) for carbonate aggregate reinforced concrete is,

$$\text{For } 273.15 \leq T \leq 673.15 \text{ degrees Kelvin}$$

$$C_{rc} = \frac{(2.566 \cdot 10^6)}{\rho_c} \quad (2)$$

This equation yields a value of around 1069 J/kg\*K, if a density value of 2400 kg/m<sup>3</sup> is used. A value for the specific heat of reinforced concrete can also be derived from first

principle heat transfer equations. If the heat transfer is assumed to be an addition of a concrete portion and a reinforced steel portion the equation is represented as,

$$Q_{rc} = Q_c + Q_s \quad (3)$$

where  $Q_T$  is the total rate of heat transfer (W),  $Q_c$  is the rate of heat transfer in the concrete (W) and  $Q_s$  is the rate of heat transfer in the steel. If the following relationship that holds for solid bodies is used,

$$Q = m \cdot c_p \cdot \frac{\partial T}{\partial t} \quad (4)$$

where  $m$  is the mass of the body and  $\frac{\partial T}{\partial t}$  is the time rate of change of temperature, and  $c_p$  is the specific heat of the body. Substituting equation (4) into equation (3) and noting that the time rate of change of temperature will be the same for the steel, the concrete and subsequently for the whole body is.

$$m_{rc} C_{rc} \frac{\partial T}{\partial t} = m_c C_c \frac{\partial T}{\partial t} + m_s C_s \frac{\partial T}{\partial t} \quad (5)$$

If this equation is solved for  $C_{rc}$  and using the fact that 4% of the volume of the reinforced concrete is steel results in the following equation for a one meter cubed section of reinforced concrete,

$$C_{rc} = \frac{(0.96m^3 \rho_c C_c) + (0.04m^3 \rho_s C_s)}{0.96m^3 \rho_c + 0.04m^3 \rho_s} \quad (6)$$

where  $\rho_c$  is the density of concrete with a value of 2175 ( $\text{kg/m}^3$ ),  $\rho_s$  is the density of steel with a value of 7800 ( $\text{kg/m}^3$ ),  $C_c$  is the specific heat of concrete with a value of 1038 (J/kg K) and  $C_s$  is the specific heat of steel with a value of 440 (J/kg K). Using these

values obtained from Incropera and Dewitt [1996] the value for  $C_{rc}$  is 960.3 J/kg. This is around 10% less than the value given by the equation proposed by Lie and Kodur [1995].

The value used in the RadThermRT simulations was 1050 J/kg K.

Table 1. Typical specific heats of concrete (partially reproduced from Table 6, Rhodes [1978])

Temperature, °C	Specific Heat J/kg K
10	917
38	971
66	1038

### Thermal Conductivity

Thermal conductivity is a measure of a material's ability to conduct heat. It can be defined as the ratio of heat flux to the temperature gradient. Customary SI units for thermal conductivity are W/m-K [Rhodes, 1978]. Steel reinforcement will tend to increase the thermal conductivity of the bridge deck, preformed beams, and the barriers by a small amount. This is due to the fact that the thermal conductivity of steel is around fifty times greater than that of concrete, though it only occupies about 4% of the volume. Table 2. has some published values of thermal conductivities for carbonate aggregate concretes. The thermal conductivity of specific heat used for this thesis was 2.5W/mK.

Table 2. Thermal conductivities of carbonate aggregate concrete. Reproduced from results [Rhodes1987],[Vodak et. Al,] [T.Z. Harwathy][H.Abe, et al 1970]

Source	Thermal Conductivity (W/m*K)
Rhodes	2.3
Vodak	2.2
Harwathy	2.5
Abe et al.	2.53

### Density

Density is a measure of how much mass occupies a unit of volume. Commonly used units for density are  $\text{kg/m}^3$ . Scott Keller [personal communication 2001], a MDT civil engineer estimated that the density of the slab in the N 19<sup>th</sup> street Bridge is approximately 2400  $\text{kg/m}^3$ . This is the value used in this thesis for density of reinforced concrete.

### Thermal diffusivity

An important property in heat transfer is the thermal diffusivity of a material expressed as,

$$\alpha_{td} = \frac{k}{\rho c_p} \quad (7)$$

where  $\alpha_{td}$  is the thermal diffusivity which has units of  $\text{m}^2/\text{s}$ ,  $k$  is the thermal conductivity,  $c_p$  is the specific heat and  $\rho$  is the density of the material. Incropera and Dewitt [1996] state “The thermal diffusivity measures the ability of a material to conduct thermal energy relative to its ability to store thermal energy. Materials of large  $\alpha_{td}$  will respond quickly to changes in their thermal environment while materials of small  $\alpha_{td}$  will respond more sluggishly.”

### Surface Properties

Surface properties that may be assigned to the standard and three layer elements in RadTherm will be considered next. These surface properties are used in the radiation heat transfer relationships. For the terrain elements these values have been previously assigned

by the software programmers. These parameters include the absorptivity and emissivity of the surfaces.

### Emissivity

Emissivity is a measure of how well the surface emits thermal radiation relative to a black body. It is defined as the ratio of the radiation emitted by the surface to the radiation emitted by a blackbody at the same temperature. Incropera and Dewitt[1996] list values for concrete as between 0.88 and 0.94. The value used for this project was 0.94. Higher emissivity values will increase the rate at which a body radiates heat away.

### Absorptivity

For any material subjected to incident, radiation incident upon it there are three things which can happen to the radiative energy. It can be absorbed, reflected, or transmitted. For opaque materials no energy is transmitted. Using the conservation of energy it is possible to say,

$$\rho_r + \alpha = 1 \quad (8)$$

where  $\rho_r$  is the reflectance and  $\alpha$  is the absorptivity. The absorptivity is the ratio of absorbed radiation flux to incident flux. Reflectance or albedo is the ratio of reflected radiation flux to the total incident flux. A mean value of absorptivity for gray Portland cement concrete given by Levinson [2001] is .65, matching that given by Pomerantz et al. [1999]. This was also the value used for this thesis

Governing Equations for Heat Transfer Problem

The governing equation that drives the problem is the first law of Thermodynamics. The first law of thermodynamics or the conservation of energy for a control volume states,

$$Q - \dot{w} = \frac{\partial E_{st}}{\partial t}, \quad (9)$$

where  $Q$  is the net heat transfer rate,  $\dot{w}$  is rate of work done,  $\left(\frac{\partial E_{st}}{\partial t}\right)$  the time rate of change of the energy stored, and all terms are expressed in watts. For this case no work is done so (9) simplifies to,

$$Q = \frac{\partial E_{st}}{\partial t} \quad (10)$$

Expanding out the heat transfer rate into components for the different mechanisms yields,

$$Q_{conv} + Q_{con} + Q_{rad} + Q_{netS} = \frac{\partial E_{st}}{\partial t} \quad (11)$$

where  $Q_{conv}$  is the convection heat transfer rate,  $Q_{con}$  is the conduction heat transfer rate,  $Q_{rad}$  is the radiation heat transfer rate, and  $Q_{netS}$  is an explicit heat transfer rate that is imposed by the short wave solar energy. Due to the fact that the body is a solid, the following relation can be used [Incropera and DeWitt 1996],

$$\frac{\partial E_{st}}{\partial t} = m \cdot c_p \cdot \frac{\partial T}{\partial t} \quad (12)$$

where  $m$  is the mass of the body in kilograms and  $c_p$  is the specific heat of the body and  $(\frac{\partial T}{\partial t})$  is the time rate of change of temperature in the body. Combining equation (11) and (12) yields,

$$m \cdot c_p \cdot \frac{\partial T}{\partial t} = Q_{conv} + Q_{con} + Q_{rad} + Q_{netS} \quad (13)$$

which is the governing equation RadTherm uses for its energy balance.

### Heat and Mass Transfer Principles

Heat transfer is energy in transit due to a temperature difference [Incrovia, 1996 pg2]. As implied above the important modes of heat transfer in the model are conduction, convection, net longwave radiation heat exchange between surfaces and the solar radiation.

#### Conduction

Conduction heat transfer is the transfer of energy from particles with more energy to ones with less energy. In general, the conduction heat transfer follows Fourier's law, which for one dimension through a plane wall is,

$$Q_x = -k \cdot A \cdot \frac{dT}{dx}, \quad (14)$$

where  $Q_x$  (W) is the heat rate by conduction through a plane wall of area  $A$  ( $m^2$ ), this heat transfer rate is proportional to the temperature gradient  $(\frac{dT}{dx})$  in the wall, and  $k$  is the thermal conductivity (W/m-K) of the wall. This can be simplified if some assumptions

are made about the thermal conductivity and the area,  $A$ . If the thermal conductivity does not change with changing temperature and if the assumption is made that the area does not change then the following equation can be used.

$$Q_x = k \cdot A \cdot \frac{\Delta T}{L} \quad (15)$$

This is a linear relationship of Fourier's law and is the equation that RadTherm/RT uses for conduction. Conduction occurs in all of the elements in the RadTherm/RT model. The terrain elements have conduction in the direction normal to the surface and through their depth between the thermal nodes. The standard elements have conduction between the front thermal node and the back thermal node and between adjacent elements. This will be discussed in more detail in the methods section.

### Convection

Convection heat transfer can be broken up into two modes, energy transfer due to diffusion (natural convection) and energy transfer carried by the motion of the bulk of a fluid (forced convection) [Incropera and DeWitt 1996]. Generally, convection is the transfer of energy between a surface and a flowing fluid that is in contact with the surface. Transfer by diffusion is usually much smaller than the energy exchange due to transfer by bulk motion. RadTherm/RT therefore neglects diffusive energy transfer. The governing equation of convection is Newton's law of cooling which can be expressed as,

$$Q = A \cdot h(T_\infty - T_s) \quad (16)$$

where the heat transfer  $Q$  is positive if it is into the surface of area  $A$ . The proportionality constant  $h$  is the convection heat transfer coefficient ( $W/m^2 \cdot K$ ). Incropera and DeWitt

[1996] state that the coefficient depends on the conditions of the boundary layer, which are influenced by surface geometry, the nature of the fluid motion, and an assortment of fluid thermodynamic and transport properties.  $T_{\infty}$  represents the bulk temperature of the fluid and  $T_s$  is the temperature of the surface. RadTherm has three options for calculating this coefficient for wind models in natural environments; low turbulent intensity, linear convection, and power law convection. Each of these options will be described in more detail in the methods section. It is up to the user to decide which option is the best to use for the application.

### Radiation Heat Transfer

Radiation heat transfer does not require a medium to carry the energy, in fact it is most efficient in a vacuum [Incropera and DeWitt 1996]. The mechanism of energy transport can be viewed as the propagation of electromagnetic waves, or as propagation of quanta or photons [Siegel, et al., 1992]. Both methods generally arrive at the same formal equations and for this project the electromagnetic wave theory was used. Thermal radiation is emitted from excited particles and differs only from other forms of electromagnetic waves in that the particles are thermally excited. All electromagnetic waves can be characterized by a spectrum of wavelengths  $\lambda$  and frequencies  $\nu$  expressed as [White,1991],

$$c = \lambda \cdot \nu, \quad (17)$$

where  $c$  is the speed of light. The electromagnetic wavelength spectrum encompasses a wide range of wavelengths from around  $10^{-5}$  to  $10^4$   $\mu\text{m}$  [White 1991]. The thermal radiation range of the spectrum is generally characterized in the range of  $10^{-1}$  to  $10^2$   $\mu\text{m}$ ,

which contains a small portion of the ultraviolet, the entire visible region, and the infrared spectrum, as shown in Figure 7.

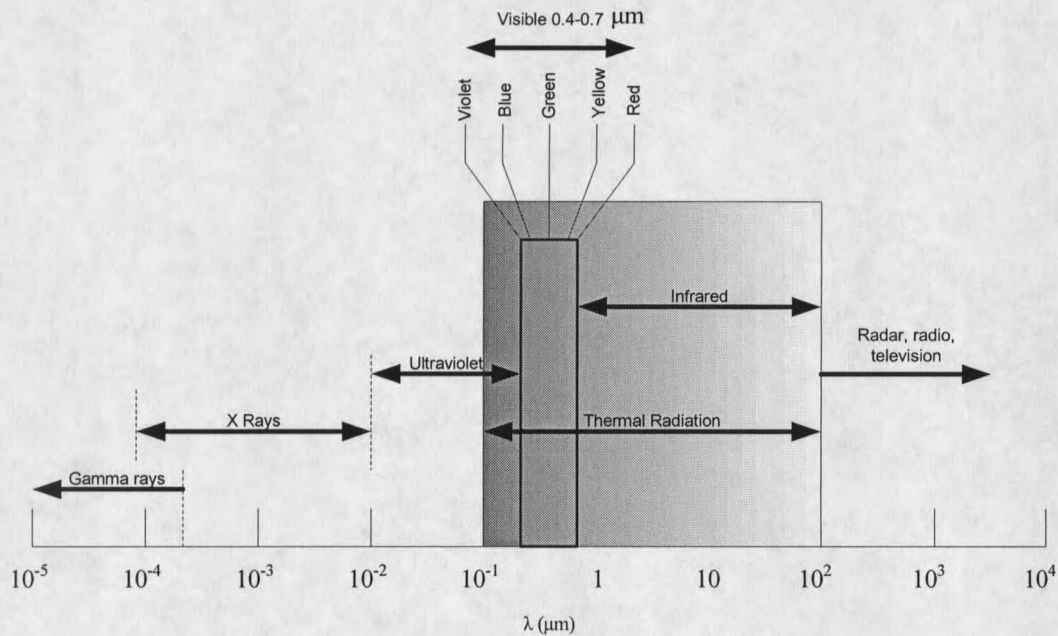


Figure 7. Spectrum of electromagnetic radiation highlighting thermal region (values from Incropera and Dewitt [1996]).

All solid opaque bodies emit thermal radiation, in addition they can absorb incident radiation or reflect incident radiation or any combination of absorbing and reflecting. A perfect emitter is termed a “blackbody”. A perfect blackbody also absorbs all incident radiation and is a diffuse emitter. If a black body has an area  $A$  and an absolute temperature  $T_s$ , its radiant emissive power is given by [White, 1991]

$$E_b = \sigma \cdot A \cdot T_s^4, \quad (18)$$

where  $E_b$  is the emitted radiation in watts,  $\sigma$  is a fundamental constant called the Stefan-Boltzmann constant, equal to  $5.67 \times 10^{-8} \text{ (W/m}^2 \cdot \text{K}^4)$ ,  $A$  is area in  $\text{m}^2$ , and  $T_s$  is in Kelvin.

Real surfaces are not black bodies and emit thermal energy at some rate lower than a black body which can be estimated [Incropera, et al. 1996] as,

$$E_r = \varepsilon \cdot \sigma \cdot A \cdot T_s^4, \quad (19)$$

where  $E_r$  is the rate that the real surface emits radiant energy, and  $\varepsilon$  is a radiative property of the surface, called emissivity. Surface emissivities have a value between zero and one. This property is a measure of how well the surface emits thermal radiation compared to a black body. This property is strongly dependent on surface material and its finish.

According to Incropera and Dewitt [1996] for radiation exchange between a small surface at  $T_s$  and a much larger isothermal surface at  $T_{sur}$  that surrounds the smaller surface, the larger surface is assumed to have blackbody emission and the smaller surface is assumed to be a gray body where the following equality holds for the small surface,

$$\alpha = \varepsilon. \quad (20)$$

Then the net rate of radiation,  $Q_r$  (W), from the smaller surface is [Incropera, DeWitt 1996]

$$Q_r = \varepsilon \cdot A \cdot \sigma (T_s^4 - T_{sur}^4) \quad (21)$$

This equation expresses the difference between the amount of thermal radiation released by emission and that, which is gained through absorption.

### Radiation View Factors

Radiation view factors are used to solve radiation heat transfer problems where radiant exchange is occurring between two or more surfaces. They are used to express the geometric relationship of how the surfaces "view" each other. If the following

assumptions are made about the surfaces, the problem can be greatly simplified; 1) emitted and reflected energy are uniform over the each surface, 2) reflected energy is diffuse, 3) emissivity and absorptivity are equal and uniform over the surface and 4) temperature is uniform over the surface [Siegel, Howell 1992]. If these assumptions are made the equation for calculating the view factor between two finite areas reduces to,

$$F_{1-2} = \frac{1}{A_1} \int_{A_1} \int_{A_2} \frac{\cos \theta_1 \cdot \cos \theta_2}{\pi \cdot S^2} dA_2 dA_1, \quad (22)$$

where  $F_{1-2}$  is the fraction of the energy leaving area  $A_1$  that arrives at area  $A_2$ , displayed graphically in Figure 8.

In a similar manner the fraction of energy that leaves area  $A_2$  and arrives at area  $A_1$  is.

$$F_{2-1} = \frac{1}{A_2} \int_{A_2} \int_{A_1} \frac{\cos \theta_1 \cdot \cos \theta_2}{\pi \cdot S^2} dA_2 dA_1, \quad (23)$$

This leads to a reciprocity relation for the view factors which is derived by the fact that the integrals in the two equations are identical, thus

$$A_1 F_{1-2} = A_2 F_{2-1}. \quad (24)$$

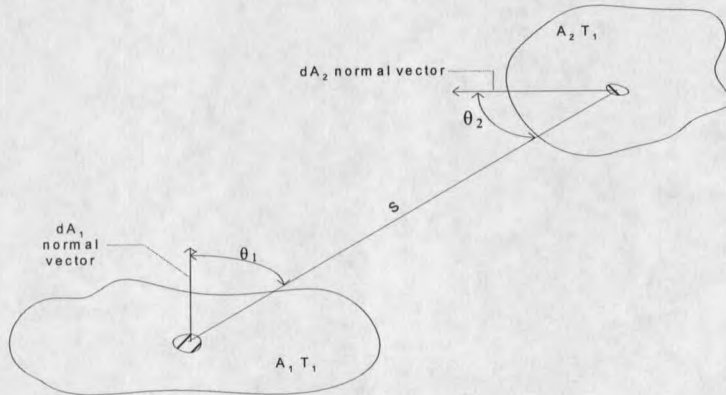


Figure 8. Geometry for exchange between finite areas (adapted from Siegel and Howell [1992]).

### Enclosure Theory

Enclosure theory considers a set of areas that are completely enclosed, such as in Figure 9. Thus the radiation leaving one surface must be absorbed or reflected by another surface. If the same assumptions are used as those in the view factor section, all radiation contributions must be accounted for. The amount of energy that leaves one surface and arrives at another is dependent on the view factors. In an enclosure with  $N$  surfaces, if energy leaves one surface then fractions of that energy must eventually reach each of the other surfaces that “view” it and the total of the fractions must be unity [Siegel, Howell 1992], that is

$$F_{k-1} + F_{k-2} + \dots + F_{k-k} + \dots + F_{k-N} = 1, \quad (25)$$

where  $F_{k-k}$  is a self view factor for concave surfaces. It is up to the modeler to decide how to break up the surfaces, more surfaces increase accuracy but add complexity.

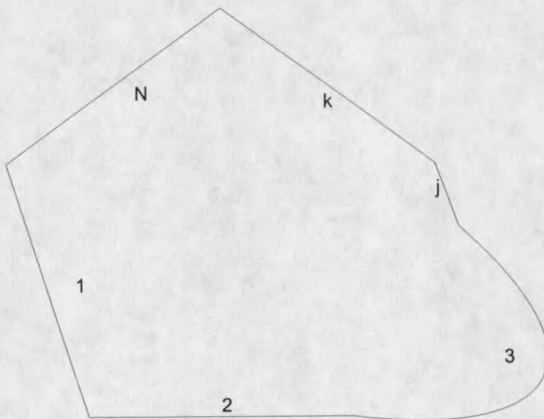


Figure 9. Example enclosure with  $N$  surfaces.

A typical heat balance for a single surface  $k$ , with area  $A_k$  inside the enclosure is [Siegel, Howell 1992]

$$Q_k = (q_{o,k} - q_{i,k})A_k, \quad (26)$$

where  $Q_k$  can be seen as either a heat transfer rate applied to the surface or as the net radiative loss from the surface to the enclosure,  $q_{o,k}$  is the emitted plus the reflected radiant energy, and  $q_{i,k}$  is the incident radiant energy from other elements in the enclosure, see Figure 10. The term  $q_{o,k}$  can be expressed as, [Siegel, Howell 1992]

$$q_{o,k} = \varepsilon_k \sigma T_k^4 + (1 - \varepsilon_k) q_{i,k}, \quad (27)$$

where the first part of the equation on the right side of the equal sign is the emitted portion and the second part is the reflected portion. The incident flux  $q_{i,k}$  is arrived at by summing the portions of energy which are emitted from  $N$  number of surfaces in the enclosure. This results in the following equation [Siegel, Howell 1992]

$$q_{i,k} = \sum_{j=1}^N F_{k-j} q_{o,j} \quad (28)$$

where the  $F_{k-j}$  are the view factors and  $q_{o,j}$  are the outgoing radiative terms from the other areas. Substituting (28) into (26) and noting that  $\sum_{j=1}^N F_{k-j} = 1$ , results in,

$$Q_k = A_k \sum_{j=1}^N F_{k-j} (q_{o,k} - q_{o,j}). \quad (29)$$

In this equation all of the incoming (i) terms have been eliminated. By substituting (27) into (26) a second simultaneous equation, where the incoming terms are eliminated is,

$$Q_k = \left[ \frac{\varepsilon_k}{1 - \varepsilon_k} (\sigma T_k^4 - q_{o,k}) \right] A_k \quad (30)$$

These two equations, (29) and (30), provide two simultaneous equations that can be written for each  $N$  surfaces. This provides  $2N$  equations with  $2N$  unknowns, with either the  $Q_k$  or the  $T_k$  being unknown, which is dependent on the boundary conditions. If however (30) is solved for  $q_{o,k}$  and substituted into (29) the following equation results, [Siegel, Howell 1992]

$$\sum_{j=1}^N \left( \frac{\delta_{kj} - F_{k-j}}{\varepsilon_j} \right) \frac{Q_j}{A_j} = \sum_{j=1}^N (\delta_{kj} - F_{k-j}) \sigma (T_k^4 - T_j^4) \quad (31)$$

Where  $\delta_{kj}$  is the Kronecker delta defined as,

$$\delta_{kj} = \begin{cases} 1 & \text{When } k = j \\ 0 & \text{When } k \neq j \end{cases} \quad (32)$$

Expanding equation (31) and solving for  $Q_k$  results in the governing equation for enclosures used in this project and in RadTherm/RT, [Marttila, 1999]

$$Q_{radk} = \frac{A_k \varepsilon_k}{1 - F_{k-k} (1 - \varepsilon_k)} \sum_{j=1}^N F_{k-j} \sigma (T_k^4 - T_j^4) + \sum_{j=1}^N \frac{Q_j}{A_j} \left[ (1 - \delta_{kj}) F_{k-j} \left( \frac{1 - \varepsilon_j}{\varepsilon_j} \right) \right], \quad (33)$$

where  $Q_{radk}$  is the net radiative loss from surface  $k$ . This provides for  $N$  equations with  $N$  unknowns where either the temperatures or the radiative losses must be known.

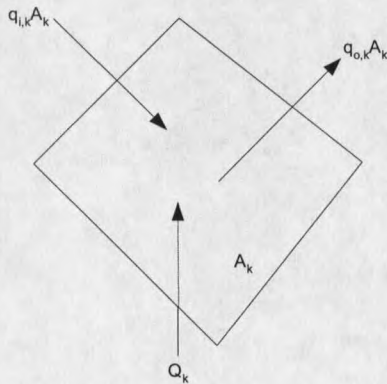


Figure 10. Radiative terms on surface area  $A$ .

### Solar Radiation

The flux of solar radiation on an exposed surface consists of that due to the direct solar beam, that due to diffuse skylight and portions of reflected radiation from other surfaces [Temps et al 1977]. The portion of the electromagnetic spectrum that includes solar radiation is; an infrared region, visible region and a portion of the ultraviolet, this is shown in Table 3. As indicated in Table 3, the ultraviolet portion does not have a significant influence on the energy balance at the surface of the earth and RadTherm does not utilize data from this wavelength. Also no attempt was made to measure UV radiation. The values for solar radiation are measured values and used as inputs into the RadTherm/RT model. The wavelengths between 0.4 to 1.2  $\mu\text{m}$  represent the shortwave region that is measured by the pyranometers. The instrument accounts for the unmeasured regions if it has been calibrated to an instrument that can measure the whole shortwave region [Licor Manual, 1986].

Table 3. Shortwave radiation definitions (Touloukian and Dewitt[1972] and Plüss [1997]).

Wavelength ( $\mu\text{m}$ )	Region	Mean radiation energy at the earth surface
0.2-0.4	Ultraviolet (UV)	9%
0.4-0.75	Visible (VIS)	49%
0.75-5.0	Near Infrared	42%

## METHODOLOGY

The first section of this chapter describes the computer models developed. Experimental methods and data formatting are discussed in the second section.

### Rhino3D Model

In this section the two geometry models are discussed. The bridge model had three different meshes derived from the same geometry. There was only one terrain model used throughout. Rhino is a surface-modeling program that is well suited to use in conjunction with RadTherm. RadTherm requires the geometry of the problem to be discretized into a mesh consisting of triangular and/or quadrilateral elements. Rhino has meshing capabilities and the meshed geometry created by Rhino can be imported seamlessly into RadTherm. The geometries of the bridge and the surrounding terrains were done separately to ease in the drawing and to help give more control over mesh development. Figure 11 shows the mesh created for the surrounding terrain, and Figure 12 shows the different bridge meshes. There were three different bridge meshes used in the analysis of the RadThermRT software, they are named using the order of magnitude of the number of elements in each bridge mesh, thus they are named; 10 element bridge mesh, 300 element bridge mesh and the 3000 element bridge mesh.

### Bridge Models

The geometry of the bridge was drawn in Rhino3D. There were no original computer aided drawings (CAD) of the bridge available. Consequently the original blue print plans

were used to model the bridge. In future projects it would be highly beneficial to use CAD drawings of the original structures. This would ensure that the geometry used in RadTherm/RT accurately reflected the true environment.

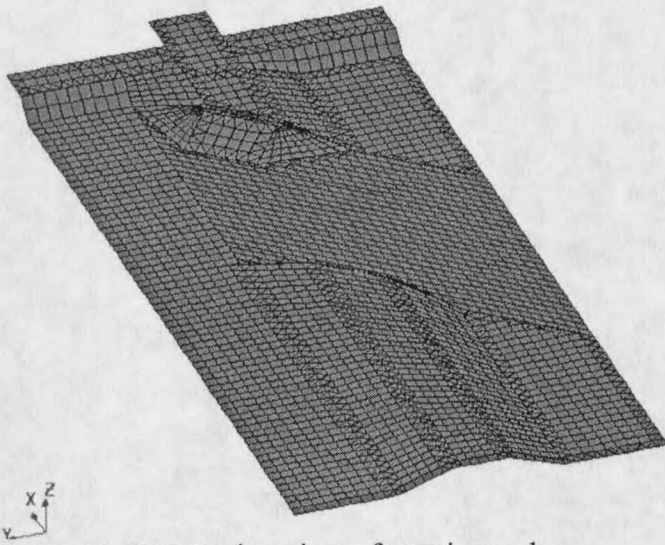


Figure 11. Perspective view of terrain mesh.

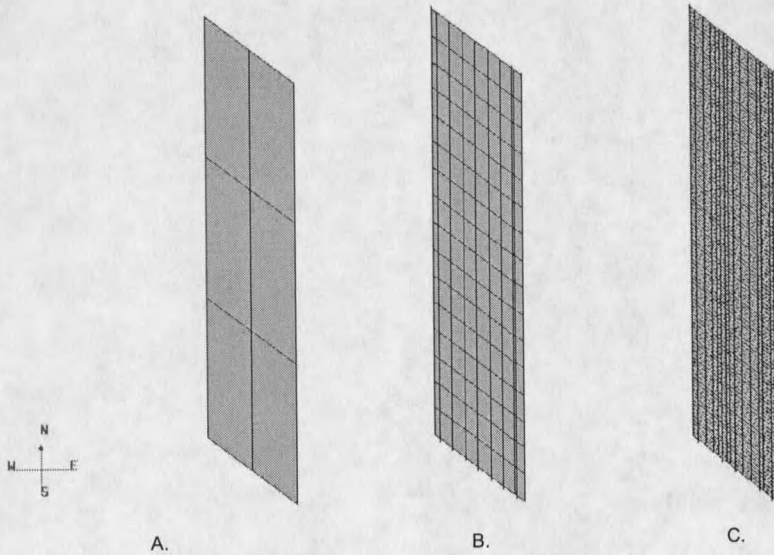


Figure 12. Top view of bridge meshes, (A) is the 10 elements bridge mesh, (B) is the 300 elements bridge mesh and (C) is the 3000 elements bridge mesh.

The bridge surface model was constructed in a deliberate and orderly fashion. First the outline of the bridge deck was drawn using the polyline command. A polyline is a line with vertexes connecting each straight section as shown in Figure 13. Polylines used for the bridge are only two vertex lines, thus to draw a square four separate polylines would be used. Next polylines were drawn, on the bridge surface along the centerlines of the support structures and barriers. This served two purposes, one to help in drawing the support structures and also to allow for individual areas to be created on the surface of the bridge between the supports. These separate areas were necessary for proper meshing and vertice alignment. After that the outline of the support structures and barriers were drawn, also using polylines. Then areas were defined for each section of bridge deck between supports and for each support and barrier using the “Create surface from curve network command” This type of surface when meshed results in only quadrilateral elements.

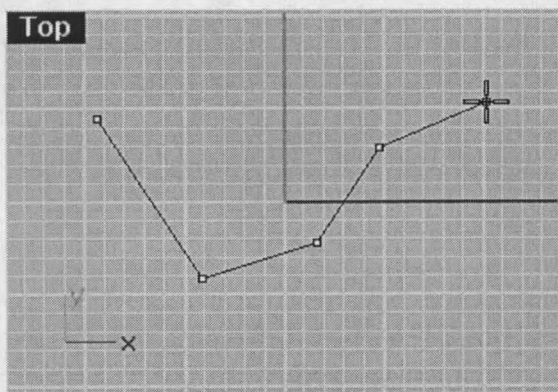


Figure 13. Example of a Rhino3D polyline with several vertices.

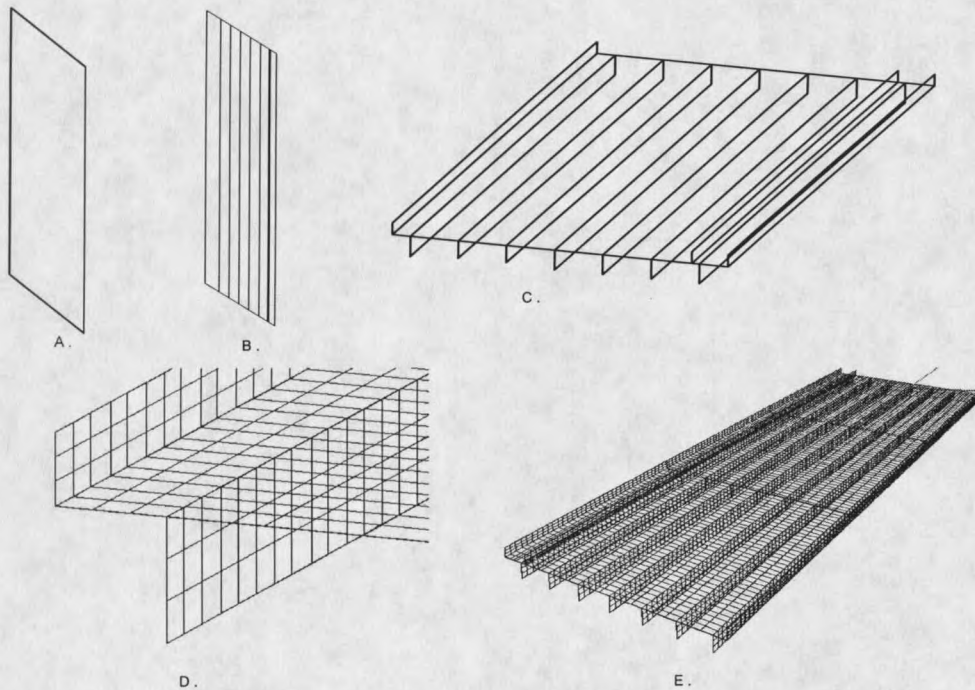


Figure 14. Steps in creation of 3000 elements bridge mesh , (A) bridge outline is drawn using polylines, (B) polylines are drawn where supports will be, (C). polylines drawn around outline of supports and barriers, (D). close up of mesh showing aligned vertices, (E) perspective of 3000 elements bridge mesh.

In order for the model to work more efficiently in RadTherm some simplifications were made. The supports of the bridge are preformed concrete I beams, these I beams are modeled as flat plates with the same volume. The model uses the same height as the actual beam and then a uniform thickness was computed to make the support beams have the same volume as the actual beams. The thickness was used in RadTherm to accurately model the beam. Figure 15 shows how the simplification is represented. A similar simplification was used for the support structures.

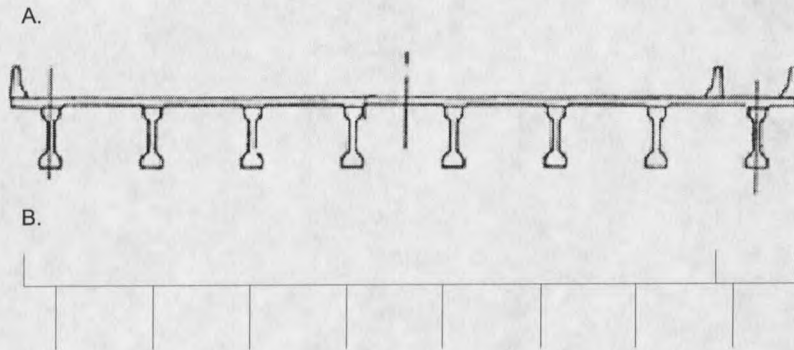


Figure 15. Cross section view showing simplification made on supports and barriers, (A) is from bridge blue prints and (B) is the cross section of modeled bridge.

Finally the areas were meshed using Rhino's Polygon Detailed Mesh Options, see Figure 16 Rhino Polygon Detailed Mesh Options. By using the Min edge length and max edge length options a clean looking mesh was created with quadrilaterals of relatively constant area was created. The Max edge length value is approximately the maximum edge length of the quads in the initial mesh grid. This option can be used for making sure the polygons are approximately the same size. Thus this value was varied for each of the three meshes. By creating a series of areas for the surface of the bridge deck the nodes on the elements of the bridge deck were aligned with the nodes for the support and barrier structures elements. This alignment is very important for the model to run correctly in RadTherm/RT. If the mesh vertices do not line up then there is no conduction between elements, since RadTherm/RT treats unaligned vertices as insulated. For the 10 element bridge mesh all of the supports and barriers were deleted.

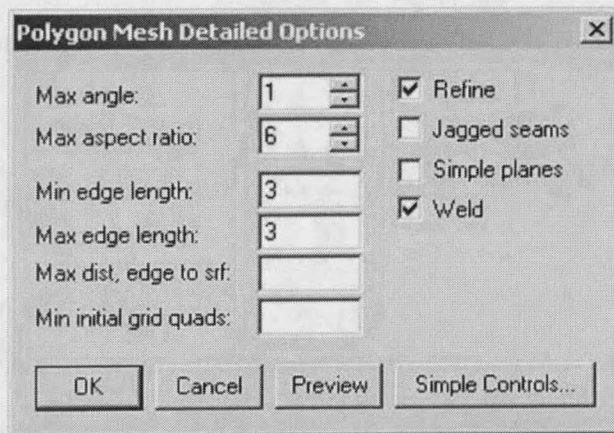


Figure 16. Polygon mesh detailed options from Rhino3D.

### Terrain Mesh

The area surrounding the bridge consists of built up embankments supporting the bridge over I-90 and ramps to allow access from the Interstate to N. 19<sup>th</sup> Ave. The embankments were drawn as flat plates as were the bridge abutments. The mesh of the surrounding areas was made to have elements that were around 10 m<sup>2</sup>. See Figure 11 for a perspective view of the terrain mesh.

### RadTherm/RT Thermal Analysis Software

RadTherm/RT is a thermal modeling package which uses a finite difference forward time stepping spatially implicit code. It also has an embedded graphical user interface. The version used in this thesis is RadTherm/RT where the RT stands for road temperature. This version of RadTherm has built in “terrain” definitions. In addition to modeling roads or terrain, it is also possible to model objects. This can include buildings, vehicles or, as in this project, a highway bridge. RadTherm/RT has several different

element part types; standard, highly conductive; three layer, terrain, and transparent. Each mesh polynomial is defined by using these element part types. Only the standard, three layer, and terrain objects were used in this project, thus the discussion will be limited to these three. Complex geometries must be imported into RadTherm/RT from some other program. In this project all geometries were created and meshed in Rhino3D. Because the model was built using two different geometry files, the imported geometries had to be oriented and aligned with each other. Proper orientation is critical in RadTherm/RT because of the solar loading and shadowing. Near components that generate shadows, a bridge running east to west may have very different solar loads than one running north to south. The orientation adjustment is done by first selecting the parts that need to be oriented. Then select the Geometry tab and the sub tab Edit and use the Translate and Rotate operations. The mesh is given default part definitions, to modify the part definitions first decide how the domain of the mesh should be divided into definitions. To apply definitions to the mesh, first select all of the elements that will be in the part. For example elements that correspond to the Interstate were chosen to be a separate part. Then on the Editor Tab click the new part button. Next the selected elements are assigned to a new part. After that the part is named using the Parts tab. If the part type is a standard or three layer type, then the user can define: material type, surface condition, and convection model to be used. The material type defines the specific heat of the material, the density of the material and the thermal conductivity. The surface definition includes the absorptivity and emissivity of the surface. If the part type is a terrain then RadTherm offers eight adjustable terrain types: Asphalt Model, Concrete Model, Foliage Model,

Layered Model, Snow Model, Soil Model, Swamp Model and Water Model. Each of these categories has sub categories. Continue assigning part definitions until all of the elements have the desired definition.

For the bridge model the surrounding terrain was imported first. All of the terrain definitions were then assigned, including a grass portion, interstate asphalt portion and highway asphalt portion. Next the Bridge geometry was imported. Using translate and rotate commands the bridge was oriented and aligned with the terrain. Then part definitions were assigned to the bridge deck sections, the support beams, and the concrete barriers. In the Rhino section the alignment of the mesh vertices was discussed. Unfortunately Rhino may not absolutely align all of the vertices; they may be separated by a small amount. To see if there are unaligned elements vertices click on View and then free edges. The free edges will be displayed in red and represent edges where no conduction takes place. If there are edges that should be aligned but are showing up as free edges, then the a condense operation can be used, this function is located in the geometry tab under the edit sub tab. There is a blank box called Max Vertex Separation, this condense command will align vertices that are closer than the Max Vertex Separation. Thus using a small value for the Max Separation, around .1 mm, all vertices should then be aligned properly. The previous red edges should now show up as yellow, indicating that there is alignment between three or more vertices, and conduction is enabled between adjacent nodes.

## Governing Equations RadTherm RT

### Standard Elements

Each standard element in the mesh has two surfaces, a front and a back surface with one temperature node assigned to each surface, as shown in Figure 17. These surfaces are separated by a user-defined thickness. Each thermal node is associated with a surface and with one-half of the volume that is bounded by the two surfaces. A single temperature is assumed for each thermal node and the volume that node occupies. Figure 18. shows all of the heat transfer modes accounted for in a standard element. The governing equation for the radiation heat transfer modes is Equation (13), restated here for convenience,

$$m \cdot c_p \cdot \frac{\partial T}{\partial t} = Q_{conv} + Q_{con} + Q_{rad} + Q_{nets} \quad (34)$$

The  $Q_{con}$ , and  $Q_{conv}$  can be further expanded using the relationships shown in equations (15) and (16) and for a specific thermal node k will result in,

$$m_k c_p \frac{\partial T_k}{\partial t} = h_k A_k (T_f - T_k) + \sum_{j=1}^{N_{cond}} \left( -k_{kj} A_{kj} \frac{T_k - T_j}{L_{kj}} \right) + Q_{rad_k} + Q_{nets_k} \quad (35)$$

where  $h_k$  is the convection coefficient,  $A_k$  is the surface area exposed to convection,  $A_{kj}$  is the cross sectional area between elements k and j,  $T_f$  is the temperature of the fluid that is convecting heat to or away from  $A_k$ ,  $N_{cond}$  is the total number of conduction links between node k and all adjacent nodes,  $k_{kj}$  is the thermal conductivity of the material between thermal nodes j and k and  $L_{kj}$  is the geometric distance between node k and node j.

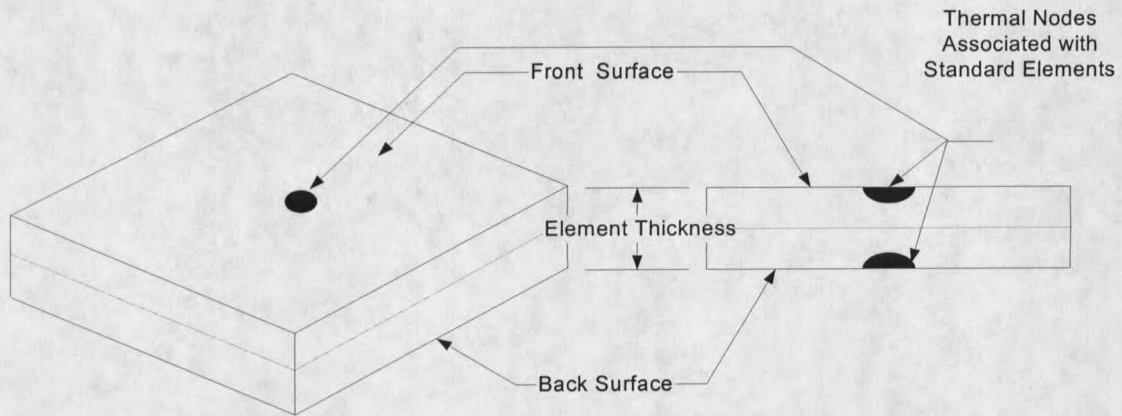


Figure 17. Standard element.

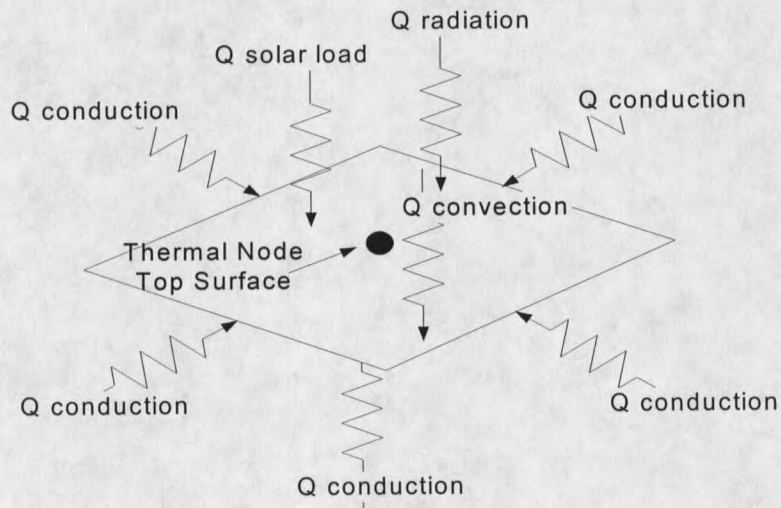


Figure 18. Heat transfer modes into standard element.

The  $Q_{netSk}$  term is an explicit term involving the amount of solar radiation node  $k$  is receiving, expressed as,

$$Q_{nets,k} = Q_{solar,k} + Q_{ref\_in,k} - Q_{ref\_out,k} \quad (36)$$

where  $Q_{solar,k}$  is the amount of solar radiation into node k,  $Q_{ref\_in,k}$  is the amount of solar radiation which is reflected into element k from all other elements and the default background element and  $Q_{ref\_out,k}$  is the amount of solar radiation which is reflected out from node k.  $Q_{solar,k}$  is defined as

$$Q_{solar,k} = \alpha_k Q_s A A_k V F_k, \quad (37)$$

where  $\alpha_k$  is the absorptivity of node k,  $Q_s$  is the total amount of solar radiation received including direct and diffuse solar radiation,  $A A_k$  is the apparent area that the radiation sees and  $V F_k$  is a visibility factor used for shadowing. The reflected radiation is solved using an iterative algorithm, first some initial guess is made for  $Q_{ref\_out,k}$  for each node k, then  $Q_{ref\_in,k}$  is calculated for each node k.  $Q_{ref\_in,k}$  depends on the guess for  $Q_{ref\_out,k}$ , and a better estimate for  $Q_{ref\_out,k}$  is calculated, it is just the reflected  $Q_{ref\_in,k}$ . This process is repeated until some  $Q_{ref\_in,k}$  minus  $Q_{ref\_out,k}$  converges to some tolerance. [Personal communication A. Curran]

The  $Q_{radk}$  term in equation (35) is obtained from the net-radiation enclosure equation (33). The term  $Q_{radk}$  is equal to the negative of  $Q_k$  in equation (33). Solving equation (35) for  $Q_{radk}$  and substituting in the value for  $Q_k$  results in the following equation,

$$\begin{aligned} & \frac{A_k \varepsilon_k}{1 - F_{k-k} (1 - \varepsilon_k)} \sum_{j=1}^N F_{k-j} \sigma (T_k^4 - T_j^4) + \sum_{j=1}^N \frac{Q_j}{A_j} \left[ (1 - \delta_{kj}) F_{k-j} \left( \frac{1 - \varepsilon_j}{\varepsilon_j} \right) \right] \\ & = -m_k c_p \frac{\partial T_k}{\partial t} + h_k A_k (T_f - T_k) + \sum_{j=1}^{N_{cond}} \left( -k_{kj} A_{kj} \frac{T_k - T_j}{L_{kj}} \right) + Q_{nets_k} \end{aligned} \quad (38)$$

This is the governing equation for the standard and three layer elements and is solved simultaneously over the domain of the problem, where  $N$  is the total number of surfaces, and  $N_{\text{cond}}$  is the total number of conduction links.

In order to solve the preceding equation some numerical iteration scheme must be used. RadTherm/RT uses a Crank-Nicholson implicit finite difference scheme. Crank-Nicholson is unconditionally stable and is second order accurate in time and space [Tannehill et al 1997]. Applying this to equation (38) and linearizing the  $T^4$  terms by the relationship in equation (39), yields equation (40)[Martilla 1999],

$$\begin{aligned}
 (T_k^4 - T_j^4) &= (T_k^2 - T_j^2)(T_k + T_j), \tag{39} \\
 -m_k C_{pk} \frac{(T'_k - T_k)}{\Delta t} &+ h_k A_k \left( \frac{T'_f + T_f}{2} - \frac{T'_k + T_k}{2} \right) \\
 + \sum_{j=1}^{N_{\text{con}}} \frac{k_{kj} A_{kj}}{L_{kj}} &\left( \frac{T'_j + T_j}{2} - \frac{T'_k + T_k}{2} \right) + \frac{Q'_{\text{nets}_k} + Q_{\text{nets}_k}}{2} \\
 &= \frac{A_k \varepsilon_k}{1 - F_{k-k} (1 - \varepsilon_k)} \sum_{j=1}^N F_{k-j} \sigma (T_k^2 - T_j^2) (T_k + T_j) \left( \frac{T'_k + T_k}{2} - \frac{T'_j - T_j}{2} \right) \\
 &+ \sum_{j=1}^N \frac{Q_j}{A_j} \left[ (1 - \delta_{kj}) F_{k-j} \left( \frac{1 - \varepsilon_j}{\varepsilon_j} \right) \right] \tag{40}
 \end{aligned}$$

The primed terms represent values from the current time step, the non primed terms represent values from the previous time step. Equation (40) can be put in a more convenient form by multiplying through by two,

$$\begin{aligned}
& -2m_k C_{pk} \frac{(T'_k - T_k)}{\Delta t} + h_k A_k (T'_j + T_j - T'_k + T_k) \\
& + \sum_{j=1}^{N_{cond}} \frac{k_{kj} A_{kj}}{L_{kj}} (T'_j + T_j - T'_k + T_k) + Q'_{nets_k} + Q_{nets_k} \\
& = \frac{A_k \varepsilon_k}{1 - F_{k-k} (1 - \varepsilon_k)} \sum_{j=1}^N F_{k-j} \sigma (T_k^2 - T_j^2) (T_k + T_j) (T'_k + T_k - T'_j - T_j) \\
& + 2 \sum_{j=1}^N \frac{Q_j}{A_j} \left[ (1 - \delta_{kj}) F_{k-j} \left( \frac{1 - \varepsilon_j}{\varepsilon_j} \right) \right]
\end{aligned} \tag{41}$$

Solving (41) for  $T'_k$  yields the final equation that is encoded in RadTherm for the numerical solution [Martilla 1999],

$$T'_k = \frac{\left[ \frac{2m_k C_{pk}}{\Delta t} T_k + \frac{A_k \varepsilon_k}{1 - F_{k-k} (1 - \varepsilon_k)} \sum_{j=1}^N F_{k-j} \sigma (T_k^2 - T_j^2) (T_k + T_j) (T'_j + T_j - T_k) \right.}{\frac{2m_k C_{pk}}{\Delta t} T_k + \frac{A_k \varepsilon_k}{1 - F_{k-k} (1 - \varepsilon_k)} \sum_{j=1}^N F_{k-j} \sigma (T_k^2 - T_j^2) (T_k + T_j) + h_k A_k + \sum_{j=1}^{N_{cond}} \frac{k_{kj} A_{kj}}{L_{kj}}} \left. + h_k A_k (T'_j + T_j - T_k) + \sum_{j=1}^{N_{cond}} \frac{k_{kj} A_{kj}}{L_{kj}} (T'_j + T_j - T_k) + Q'_{nets_k} + Q_{nets_k} - \frac{2A_k \varepsilon_k}{1 - F_{k-k} (1 - \varepsilon_k)} \sum_{j=1}^N \left[ (1 - \delta_{kj}) F_{k-j} \left( \frac{1 - \varepsilon_j}{\varepsilon_j} \right) \right] \frac{Q_j}{A_j} \right] \tag{42}$$

The outgoing radiation or  $Q_j$  terms in equation (42) are evaluated each time  $T_k$  is evaluated using equation (33). In order to solve for the temperature distribution over the domain of the problem equation (42) is written for each thermal node. This system of equations requires an iterative method. The method that RadTherm/RT uses is Successive Over Relaxation with an adjustable tolerance value, the matrix equation is solved using Gauss Elimination with partial pivoting. The iterative method is used to converge the governing equations on a solution at each time step.

### Three Layer Elements

Three layer elements are similar to the standard elements, except that for each element there are four temperature nodes and the ability to define the thickness for each layer. The conductivities are also adjustable for each layer. This is shown in Figure 19. The three layer elements have the same heat transfer modes as the standard elements and also have the same governing equation. For the interior thermal node the only available heat transfer mode is conduction. These elements were used to define the bridge deck.

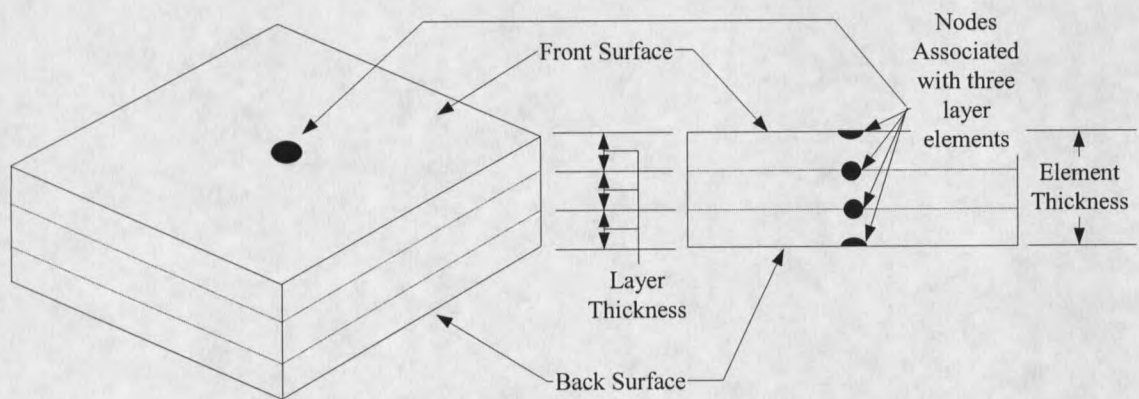


Figure 19. Three layer elements.

### Terrain Elements

There are several first principle terrain models built into RadTherm/RT including a soil model, foliage model, water model, snow model, swamp model and concrete or asphalt model. These models are used to define the terrain elements. Terrain elements used in this thesis are foliage elements and asphalt or concrete elements, thus details are

only given for these models. All of the terrain elements use multiple layers, where each layer has a thermal node; these layers are perpendicular to the surface normal in the direction of increasing ground depth. The foliage model uses a thermal node that is above ground and represents the foliage. For the interior nodes the only available mode of heat transfer is conduction between nodes above and below. The core temperature, is defined at the bottom node, and must be defined as an input into the model, as shown in Figure 20. The terrain elements take into account the physical processes of; convection between the air and ground, convection between the air and foliage, and radiation between the ground and sky, radiation between the ground and foliage, radiation between foliage and sky, conduction through ground layers, solar loading including shadowing, evaporation/condensation, and precipitation. Unlike the standard and three layer elements there is no conduction between the elements. This is reasonable as the thermal conductivity of most terrain nodes is relatively small, and the temperature is relatively constant at similar depths, thus virtually no conduction would take place in a direction perpendicular to the surface. Each first principle model uses the same governing equation as is used for the standard and three layer elements with the addition of a mass transport coefficient to track the precipitation, evaporation and condensation rates. Adding these terms yields Equation(43),

























































































































































































